UHRF1 upregulation mediates exosome release and tumor progression in osteosarcoma

Stephanie C. Wu[1,2], Ahhyun Kim[1], Loredana Zocchi[1], Claire Chen[1], Jocelyne Lopez[2], Kelsey Salcido[2], Jie Wu[3,4], and Claudia A. Benavente[1,2,4]

[1]Department of Pharmaceutical Sciences, University of California, Irvine, CA 92697, USA.

[2]Department of Developmental and Cell Biology, University of California, Irvine, CA 92697, USA.

[3]Department of Biological Chemistry, University of California, Irvine, CA 92697, USA.

[4]Chao Family Comprehensive Cancer Center, University of California, Irvine, CA 92697, USA.

Correspondence:

Claudia A. Benavente

University of California, Irvine

839 Medical Sciences Ct, Sprague Hall 108

Irvine, CA 92697, USA

Phone: 949-824-7845

E-mail: Claudia.benavente@uci.edu

ABSTRACT

Loss of function mutations at the retinoblastoma (*RB1*) gene are associated with increased mortality, metastasis and poor therapeutic outcome in several cancers, including osteosarcoma (OS). However, the mechanism(s) through which *RB1* loss worsens clinical outcome remain to be elucidated. Ubiquitin-like with PHD and Ring Finger domains 1 (UHRF1) has been identified as a critical downstream effector of the RB/E2F signaling pathway that is overexpressed in various cancers. Here, we show that UHRF1 upregulation is critical in rendering OS cells more aggressive. Using novel OS genetically engineered mouse models, we determined that knocking-out *Uhrf1* considerably reverses the poorer survival associated with *Rb1* loss. We also found that high *UHRF1* expression correlates with increased clinical presentation of metastatic disease. Based on gain- and loss-of-function assays, we found that UHRF1 promotes cell proliferation, migration, invasion, and metastasis. UHRF1-mediated cell mobility results as a consequence of altered extracellular vesicles and their cargo, including urokinase-type plasminogen activator (uPA). Our work presents a new mechanistic insight into *RB1* loss-associated poor prognosis and a novel oncogenic role of UHRF1 through regulation of exosome secretion that is critical for OS metastasis. This study provides substantial support for targeting UHRF1 or its downstream effectors as novel therapeutic options to improve current treatment for OS.

37 **INTRODUCTION**

38

39 Osteosarcoma (OS) is the most common primary cancer of bone and typically occurs in children and young
40 adults. As a highly metastatic cancer, 15-20% of OS patients are diagnosed after the cancer has already
41 metastasized (typically to the lungs), which translates to 5-year survival rates of <40% [1]. In comparison,
42 patients without metastases have survival rates of 65-75%. Unfortunately, pulmonary metastases occur
43 in nearly half of all OS patients [2]. OS survival rates have plateaued since the introduction of adjuvant
44 and neoadjuvant multiagent chemotherapy in the early 1980s [3]. Thus, there is a pressing clinical need
45 to determine the factors responsible for metastasis in OS to facilitate development of new therapeutic
46 strategies.

47

48 The most common genetic mutations found in OS are in tumor suppressors *TP53* and *RB1* [4, 5]. Loss-of-
49 function mutations of the *RB1* gene in OS are associated with poor therapeutic outcome as defined by
50 increased mortality, metastasis, and poor response to chemotherapy [6-10]. However, the mechanism(s)
51 through which RB loss leads to poor prognosis remains unclear. A previous study in retinoblastoma
52 identified Ubiquitin-like, containing PHD and RING finger domains 1 (UHRF1) as a key target gene
53 downstream of the RB/E2F signaling pathway that is abnormally upregulated following the loss of RB, and
54 contributes to tumorigenesis [11]. UHRF1 is a multi-domain protein that exerts various functions that
55 include, but are not limited to, reading and writing of epigenetic codes. UHRF1 is most known for its role
56 in maintaining DNA methylation throughout replication by recruiting DNA methyltransferase 1 (DNMT1)
57 to hemi-methylated DNA at the replication fork. In recent years, many reports have emerged showing
58 overexpression of UHRF1 in different types of human cancers that frequently present *RB1* mutations
59 including lung, breast, bladder, colorectal cancer, and retinoblastoma [11-15]. Thus, we hypothesized that

60 loss of RB in OS contributes to tumor progression and increased malignancy through upregulation of its
61 downstream target UHRF1.
62
63 In this study, we provide evidence for UHRF1 as a key player in OS tumorigenesis, promoting proliferation,
64 migration, and metastasis. Loss of *Uhrf1* in developmental OS mouse models drastically delayed tumor
65 onset, decreased pulmonary metastasis, and increased the life span of mice carrying *Rb1* mutations. We
66 identified a novel role of UHRF1 in promoting exosome secretion which is associated, at least in part, with
67 the induction of migration and invasion through the secretion of proteolytic enzymes including urokinase-
68 type plasminogen activator (uPA) to remodel the extracellular matrix. Targeting uPA with small-molecule
69 inhibitors resulted in a robust decrease in OS migration and invasion. These findings highlight a critical
70 role of UHRF1 as a driver of the poor prognosis associated with RB loss and presents UHRF1 and its
71 downstream targets as a novel therapeutic targets for OS.
72
73 **MATERIALS AND METHODS**
74
75 **Xenografts, mouse models and cell lines**
76 The five orthotopic xenografts used in this study: SJOS001105 (PDX1), SJOS001112 (PDX2), SJOS001107
77 (PDX3), SJSO010930 (PDX4), and SJOS001121 (PDX5) were obtained from the Childhood Solid Tumor
78 Network [16]. Athymic nude (NU/J) mice were obtained from The Jackson Laboratories. The *p53*^{lox} and
79 *Rb1*^{lox} conditional-knockout (cKO) mice were obtained from the Mouse Models of Human Cancer
80 Consortium at the National Cancer Institute; the *Osx-cre* mice were obtained from The Jackson Laboratory.
81 For *Uhrf1* cKO mice, mice obtained from the European Mouse Mutant Archive were backcrossed to
82 flipasse (Flp) mice for removal of the neo-cassette (tm1c conversion), and then backcrossed to C57BL/6N
83 mice for Flp removal. Mice were monitored weekly for signs of OS. Moribund status was defined as the

84 point when tumors had reached 10% body weight or induced paralysis in the mouse. The University of
85 California Irvine Institutional Animal Care and Use Committee approved all animal procedures.
86
87 OS cell lines 143B, SJSA-1, SaOS-2 and U-2 OS, as well as MSCs and HEK293T cells were acquired from
88 ATCC and maintained according to their specifications.
89
90 **FDG-PET/microCT scan**
91 Overnight-fasted mice were injected with 0.1-0.5 mCi of ^{18}F-FDG in sterile saline (0.05-0.2 ml)
92 intraperitoneally (i.p.) and allow to uptake the ^{18}F-FDG for 60 min prior to imaging. Animals were
93 anesthetized and laid in supine position on the scanner holder with continued anesthesia. Scanning data
94 was acquired in full list mode and sorted into a single frame, 3 dimensional sinogram, which was rebinned
95 using a Fourier rebinning algorithm. The images were reconstructed using 2-dimensional filter back
96 projection using a Hanning Filter with a Nyquist cut off at 0.5 and corrected for attenuation using the Co-
97 57 attenuation scan data. Analysis of PET was conducted using PMOD 3.0 and IRW software. The PET data
98 was co-registered to the CT template for drawing regions-of-interest (ROI). The ROI data was converted
99 to standard uptake value (SUV) of ^{18}F-FDG.
100
101 **Western blotting**
102 Western blots were performed as described [17] using the following antibodies and dilutions: 1:1000 anti-
103 Uhrf1 (sc-373750, Santa Cruz Biotechnology), 1:1000 anti-Rb (9313T, Cell Signaling), anti-actin (A1978,
104 Sigma), anti-E2F1 (3742S, Cell Signaling), anti-E2F2 (sc-9967, Santa Cruz Biotechnology), anti-E2F3 (MA5-
105 11319, Nalgene Nunc). Secondary antibodies were diluted 1:1000 (PI-1000 or PI-2000, Vector
106 Laboratories). Bands were visualized using chemiluminescence (SuperSignal™ West Pico
107 Chemiluminescent Substrate, Thermo Scientific). Band intensities were analyzed using ImageJ software.

108

109 ***In situ* hybridization**

110 OS tissue microarrays were purchased from US Biomax, Inc (OS804c). 6 stage IA (T1N0M0), 16 stage IB
111 (T2N0M0), 1 stage IIA (T1N0M0), 16 stage IIB (T2N0M0) and 1 stage IVB (T2N1M0) tumors are represented
112 in the array. Stage I tumors are low grade and stage II and IV are high grade. The extent of the primary
113 tumor (T) is classified as intercompartmental (T1) or extracompartmental (T2). Tumors that have
114 metastasized to nearby lymph nodes are denoted by N1, but no distant organ metastases (M0) are
115 represented in the array. Formalin-fixed, paraffin-embedded (FFPE) slides were incubated at 60°C for 1hr
116 for deparaffinization, followed by two washes of xylene and two washes of 100% ethanol for dehydration,
117 5 min each at RT, before air-drying. RNAscope® technology was utilized for *in situ* hybridization. Assay was
118 performed following manufacturer's protocol. Human and mouse UHRF1-specific probes were
119 customized by Bio-Techne. RNAscope® Positive Control Probe- Hs-PPIB/Mm-PP1B and
120 RNAscope® Negative Control Probe- DapB were used. OpalTM 570 fluorophore was used at a 1:1000
121 dilution. Slides were mounted with ProLong Gold Antifade Mountant.

122

123 **Chromatin immunoprecipitation (ChIP assay)**

124 ChIP assays were performed as previously described [18]. ChIP DNA was analyzed by qPCR with SYBR
125 Green (Bio-Rad) in ABI-7500 (Applied Biosystems) using the following primers. For motif 1 (M1), Forward:
126 5'-CCACATTCCCTCGCAGTATTTA-3'; Reverse 5'-CCCTGAACTCTTAAGTCCAAGTC-3'; for motifs 2 and 3 (M2,
127 M3), Forward: 5'-CACCCTCTTTCTCGCTTCC-3'; Reverse 5'-TGCCAGCTGCTCTGATTT-3'. The anti-E2F1 (3742;
128 Cell Signaling) and rabbit IgG (sc-2027, Santa Cruz Biotechnologies) antibodies were used.

129

130 **Real-time RT-PCR (qPCR)**

131 We performed qPCR as described [17]. Primers were designed using IDT Real-Time PCR tool (Integrated
132 DNA Technologies). Reaction was carried out using 7500 Real-Time PCR system (Applied Biosciences).
133 Data were normalized to those obtained with endogenous control 18S mRNA and analyzed using
134 ΔΔCt method. Primer sequence for PCR amplification are as follows: *UHRF1* (5'-
135 GCTGTTGATGTTTCTGGTGTC-3'; 5'-TGCTGTCAGGAAGATGCTTG-3'), *PLAU* (5'-
136 GAGCAGAGACACTAACGACTTC-3'; 5'-CTCACACTTACACTCACAGCC-3'), *SEMA3E* (5'-
137 CTGGCTCGAGACCCTTACTG-3'; 5'- CAAAGCATCCCCAACAAACT-3'), *HAS2* (5'-TCCATGTTTTGACGTTTGCAG-
138 3'; 5'-AGCAGTGATATGTCTCCTTTGG-3'), *LAMC2* (5'-CACCATACTCCTTGCTTCCTG-3'; 5'-
139 GTGCAGTTTGTCTTTCCATCC-3'), *18S* (5'-GTAACCCGTTGAACCCCATT-3'; 5'-CCATCCAATCGGTAGTAGCG-3').
140

141 **Lentivirus production and transduction**

142 Lentiviral particles were produced by co-transfecting the envelope plasmid pCMV-VSV-G (Addgene),
143 packaging plasmid pCMV-dR8.2 dvpr (Addgene), lentiCRISPRv2 (Addgene) or plentiCRISPRv2 (GenScript)
144 with UHRF1 gRNA (gRNA sequence: TCAATGAGTACGTCGATGCT), inducible CRISPR/Cas9 plasmid TLCV2
145 (Addgene plasmid #87360) with UHRF1 gRNA (gRNA1 sequence: CGCCGACACCATGTGGATCC and gRNA2
146 sequence: ACACCATGTGGATCCAGGTT) into HEK293T cells using calcium phosphate transfection method.
147 Supernatants containing lentiviral particles were harvested at 24 h and 48 h post-transfection. Cell debris
148 were cleared by centrifugation at 1600 × g for 10 min at 4°C. Supernatants were then filtered through 0.45
149 µm PES filter (25-223, Genesee Scientific), and concentrated by ultracentrifugation at 23000 RPM for 2 h
150 at 4°C. Lentiviral particles were resuspended in ice-cold PBS and stored at -80°C. Transduction of target
151 cells were achieved by exposing cells to viral particles in serum-free condition for 6 hr. Puromycin selection
152 was carried out at a concentration of 2 µg/ml.
153

154 **Clonogenic assay**

155 6-well plates were coated with 1ml of 0.75% agarose prior to seeding. Single cell suspension was mixed
156 with agarose to achieve a final agarose concentration of 0.36%, the mixture was then layered on top of
157 the 0.75% agarose coating (Seeding density 200 cells/cm^2). Cells were incubated at 37°C with 5% CO_2 until
158 cells in control wells have formed sufficiently large colonies (>50 cells). Colonies were fixed with 10%
159 methanol for 15 min and stained with 5% Giemsa for 30 min for visualization.
160

161 **Immunocytochemistry**

162 Cell were seeded onto glass coverslips in a 24-well plate at a density of 25000 cells/well and allowed to
163 attach overnight. For EdU staining the Click-iT EdU cell proliferation kit (Thermo Fisher Scientific) was used
164 following manufacturer's instructions with 1 h pulse using a final 10 µM EdU solution in media. For UHRF1
165 immunostaining, media was aspirated, and cells were fixed using 4% (w/v) paraformaldehyde overnight
166 at 4°C. Slides washed with PBS twice and then incubated with primary antibody overnight at 4°C. Mouse
167 anti-UHRF1 antibody (PA5-29884, Thermo Fisher Scientific) was used at 1:500 dilution. Slides washed 3
168 times in PBS then incubated with anti-rabbit secondary antibody (BA-1000, Vector Laboratories) at 1:500
169 dilution with corresponding blocking buffer for 30 min at RT in the dark. Slides were washed 3 times with
170 PBS and incubated in 300 µl of Vectastain ABC kit (Vector Laboratories) for 30 min at RT. Slides were
171 washed 3 times in PBS and incubated with tyramide Cy3 1:150 in amplification buffer (Perkin Elmer) for
172 10 min. After washing with PBS for 3 times, DAPI was added (1:1000 dilution in PBS) for 5 min to stain the
173 nuclei. Slides were washed twice with PBS and mounted using gelvatol containing DABCO. Imaging was
174 completed using Life Technologies EVOS microscope. Cell scoring was performed by a blinded investigator.
175

176 **Subcutaneous injection**

177 Human OS cell lines were dissociated in 0.25% trypsin-EDTA, washed with PBS prior to counting. $2 \cdot 10^6$
178 cells were resuspended in 100 µl of PBS and injected subcutaneously into the flank region of mice. Tumors

179 were collected 3 weeks post injection. For cells that require doxycycline induction for the expression
180 CRISPR/Cas9, 2 mg/ml doxycycline hyclate supplemented water was administered *ad libitum*. 10 mg/ml
181 of sucrose was added to doxycycline supplemented water to increase consumption.
182
183 **RNA Sequencing**
184 Total RNA was isolated using the RNA Micro Kit (Qiagen). Subsequently, 500 ng of total RNA was used to
185 create the RNA-seq library following the manufacturer's protocol from purification, mRNA fragmentation
186 through the adenylation of end-repaired cDNA fragments and cleanup (TruSeq Stranded mRNA, Illumina).
187 The collected sample was cleaned with AMPure XP beads (Beckman Coulter) and eluted in 20 µl of 10 mM
188 Tris buffer, pH 8, 0.1% Tween 20. A paired-end 100-bp sequencing run was performed on HiSeq 4000
189 yielding 348M PE reads with a final library concentration of 2 nM as determined by qPCR (KAPA Biosystem).
190
191 Sequencing reads were aligned to the mouse or human reference genome (GRCm38 or GRCh38, ENSEMBL
192 v.92) using STAR (v2.5.2a) [19]. Each read pair was allowed a maximum number of mismatches of 10. Each
193 read was allowed a maximum number of multiple alignments of 3. Gene counts for each sample were
194 produced using HTSeq (v0.6.1p1) [20]. Read count normalization and differential expression analysis were
195 performed using DESeq2 (v1.22.2) in R (v3.5.2) [21]. Genes with low reads (sum across samples < 10) were
196 removed. Differentially expressed genes (DEG) were calculated by comparing UHRF1 knockouts to
197 matching controls, genes with base mean ≥ 10, Log2FoldChange ≥ 1 or ≤ -1, and adjusted p value
198 (Benjamini-Hockberg) ≤ 0.05 were called differentially expressed genes. 3D PCA plot was generated using
199 the R package plot3D (v1.1.1).
200

201 All sequencing data discussed in this publication have been deposited in NCBI's Gene Expression Omnibus
202 [22] and are accessible through GEO Series accession number GSE144418
203 (https://www.ncbi.nlm.nih.gov/geo/query/acc.cgi?acc=GSE144418).
204
205 **Scratch-wound assay**
206 Cells were seeded the day before the scratch at a density of $1.1 \cdot 10^5/cm^2$ and grown to 100% confluency
207 in 6-well cell culture plates. 2 h before the scratch, cells were treated with 5 µg/ml of mitomycin C (S8146,
208 Sigma). At time 0, a 1000 µl tip was used to create a wound across the cell monolayer. The cells were
209 incubated for 8 h at 37°C with 5% CO_2. Images of the wound at the exact same field were taken at 0 and
210 8 h and analyzed using the ZEISS ZEN microscope software. A total of 20 measurements in pixels were
211 made per image. The pixels migrated was calculated as the difference between the average width of the
212 scratches before and after the incubation period. p-values were calculated using two-tailed t-test.
213 Amiloride was used at 150 µM, BC 11 hydrobromide at 16.5 µM, GW4869 at 10 µM, which were
214 supplemented in growth medium and given to the cells at the 0 h time point. Chlorpromazine (CPZ) was
215 used at 20 µM for 30 min prior to scratch. For experiments using conditioned media, serum-free media
216 was used and exposed to cells for 24 h.
217
218 **Transwell invasion assay**
219 8 µm pore PET membranes (353097, Corning) were coated with Matrigel (25 µg/insert). $2 \cdot 10^4$ cells were
220 seeded onto the membrane in 100 µl of appropriate cell culture medium and placed into the incubator
221 for 2 h at 37°C with 5% CO_2 to allow cell attachment. After cells have attached, 100 µl of media were
222 added to the inner chamber, amiloride (150 µM final concentration) or BC11 hydrobromide (16.4 µM final
223 concentration) or doxycycline (1 µg/ml final concentration) were supplemented at this time. 600 µl of
224 appropriate cell culture medium supplemented with 100 ng/ml fibroblast growth factor (FGF) was added

225 to the outer chamber. Cells were incubated for 16 h at 37°C with 5% CO_2. Cell culture medium was
226 aspirated, and cotton swabs were used to scrape off non-migratory cells on the top side of the insert. The
227 remaining cells at the bottom side of the insert were then fixed and stained with a solution consists of 6%
228 glutaraldehyde and 0.5% crystal violet for 2 hr. Stains were washed out with tap water and the inserts left
229 to dry at room temperature. Images of 5 different fields within each insert were taken for analysis by cell
230 count.
231
232 **Tail vein injection**
233 Human OS cells lines were dissociated in 0.25% trypsin-EDTA, washed with PBS prior to counting. For the
234 experimental metastasis model, 2×10^6 cells were resuspended in 200 µl of PBS and injected intravenously
235 through the tail vein. Mice lungs were collected 3 weeks after injection, fixed in 4% formaldehyde for
236 histological analysis.
237
238
239 **RESULTS**
240
241 **UHRF1 overexpression in mouse OS is a critical driver of the poor survival in *Rb1*-null OS**
242
243 The OS developmental mouse model using Osterix-driven Cre-recombinase (Osx-cre) to facilitate
244 preosteoblast-specific loss of *Tp53* results in OS tumor formation with complete penetrance and gene
245 expression profiles, histology, and metastatic potential comparable to that of human OS [23, 24]. Loss of
246 *Rb1* in addition to *Tp53* potentiates OS in these mice, strongly mimicking the behavior of the disease in
247 human. These OS mice develop tumors with calcified interior and highly proliferative exterior, which can
248 be captured by microCT and FDG-PET scans, respectively (Fig. 1A). Our previous work identified *UHRF1* as

249 a target overexpressed upon *RB1* inactivation that plays a significant role in the epigenetic-driven tumor
250 progression in retinoblastoma [11]. Analysis of UHRF1 expression in OS tumors arising in *Tp53* single
251 conditional-knockout (cKO; *Osx-cre Tp53*$^{lox/lox}$) and *Tp53*/*Rb1* double conditional-knockout (DKO; *Osx-cre*
252 *Tp53*$^{lox/lox}$ *Rb1*$^{lox/lox}$) OS tumors revealed UHRF1 is highly expressed both at the mRNA (Fig. 1B) and protein
253 level compared to mouse mesenchymal stem cells (mMSC; Fig. 1C).
254
255 Before examining the role of UHRF1 in OS development *in vivo*, we first assessed the effect of *Uhrf1* loss
256 in normal bone development. Since *Uhrf1* KO mice result in mid-gestational lethality [25], we generated
257 *Uhrf1* cKO mice (*Osx-cre Uhrf1*$^{lox/lox}$). Bone density analyses of the femur, tibia, and humerus exhibited no
258 difference in Hounsfield units (n=4) upon preosteoblastic loss of *Uhrf1* in either male or female mice (Fig.
259 1D-E). Thus, *Uhrf1* loss does not appear to affect normal bone development, independent of sex (Fig. 1E).
260 Then, we crossed our *Uhrf1* cKO with the developmental OS mouse models *Tp53* cKO and *Tp53*/*Rb1* DKO,
261 resulting in *Tp53*/*Uhrf1* DKO (*Osx-cre Tp53*$^{lox/lox}$ *Uhrf1*$^{lox/lox}$) and *Tp53*/*Rb1*/*Uhrf1* triple knockout (TKO; *Osx-*
262 *cre Tp53*$^{lox/lox}$ *Rb1*$^{lox/lox}$ *Uhrf1*$^{lox/lox}$). Overall survival and tumor formation of *Tp53*/*Uhrf1* DKO and
263 *Tp53*/*Rb1*/Uhrf1 TKO mice were tracked and compared to their corresponding littermate controls (*Tp53*
264 cKO and *Tp53/Rb1* DKO, respectively) to assess the role of UHRF1 in osteosarcomagenesis and metastasis.
265 All genotypes analyzed led to the development of OS in mice, but with distinct survival rates and disease
266 presentation. *In situ* hybridization performed on the OS mouse tumors confirmed a significant reduction
267 of *Uhrf1* in *Tp53*/*Uhrf1* DKO and *Tp53*/*Rb1*/*Uhrf1* TKO (Fig. 1F). In line with previous reports, the loss of
268 *Rb1* in *Tp53*/*Rb1* DKO mice resulted in a significantly shorter median survival (28.1 weeks; n=53) compared
269 to *Tp53* cKO mice (48.4 weeks; n=39, $p<0.0001$), recapitulating the poor prognosis associated with *RB1*
270 loss in humans (Fig. 1G). Strikingly, genetic ablation of *Uhrf1* in *Tp53/Rb1/Uhrf1* TKO mice resulted in a
271 significant increase in survival compared to *Tp53/Rb1* DKO mice, with a median survival of 46.9 weeks
272 (n=37; $p<0.0001$). The median survival of *Tp53/Rb1/Uhrf1* TKO (46.9 weeks) was comparable to that of

273 *Tp53* cKO (48.4 weeks, p=0.0577, Gehan-Breslow-Wilcoxon test), suggesting that elevated UHRF1 is
274 critical for the poor prognosis associated with *Rb1* loss (Fig. 1G). However, the overall survival of
275 *Tp53/Rb1/Uhrf1* TKO and *Tp53* cKO mice is distinct from each other (p=0.0126, Mantel-Cox test),
276 suggesting that early UHRF1 overexpression is not the only factor contributing to *Rb1* loss-associated
277 outcomes. Since three *Tp53/Rb1/Uhrf1* TKO mice had not acquired tumors well beyond the average of
278 the rest of their study group (> 69 weeks; Fig. 1G†), we performed FDG-PET/microCT scans on these mice,
279 followed by autopsy. FDG-PET/microCT scans revealed no detectable tumors (Supp. Fig. 1), which was
280 further confirmed through autopsy, suggesting that *Uhrf1* loss likely prevents early stages of tumor
281 initiation or tumor progression in this OS model. Most remarkably, genetic ablation of *Uhrf1* also resulted
282 in a significant reduction in pulmonary metastatic potential, with only 10% of mice presenting lung
283 metastases in *Tp53/Rb1/Uhrf1* TKO compared to 40% in *Tp53/Rb1* DKO mice. In addition to the reduced
284 metastatic incidence rate, a lighter burden of metastatic nodules was also observed in *Tp53/Rb1/Uhrf1*
285 TKO mice.
286
287 Since increased *Uhrf1* mRNA and protein levels were also detected in *Tp53* cKO mouse tumors (Fig. 1B-C),
288 we examined the effect of *Uhrf1* loss in *Tp53/Uhrf1* DKO compared to *Tp53* cKO mice. We observed a
289 significant increase in the median survival of *Tp53/Uhrf1* DKO mice (71.4 weeks; n=39), compared to *Tp53*
290 cKO (n=39; p=0.0007, Gehan-Breslow-Wilcoxon test), but not in overall survival (p=0.1189, Mantel-Cox
291 test; Fig. 1H). Interestingly, we found that all *Tp53* cKO mice analyzed with early morbidity (< 50 weeks)
292 presented tumors with increased *Uhrf1* mRNA levels, suggesting spontaneous RB pathway inactivation,
293 when compared to tumors from mice that reached moribund status later in life (> 50 weeks; Supp. Fig.
294 1B). This increased *Uhrf1* mRNA expression correlated with increased *Cdk4* expression in these tumors
295 (Supp. Fig. 1C). No correlation was found with the expression of other RB regulators, including *p16* and
296 *Cdk6*, even though the only tumor with undetectable *p16* expression was observed a young tumor (Supp.

297 Fig. 1D-E). No significant changes on *Rb1* expression were observed between these groups (Supp. Fig. 1F).
298 Pathology analysis of histological sections for tumors from the four OS mouse models analyzed linked
299 *Uhrf1* loss with lower mitotic index and decreased anaplasia (Supp. Fig. 2 and Supp. Table 1).
300
301 The observation that UHRF1 loss significantly increased overall survival in *Tp53/Rb1/Uhrf1* TKO but not
302 *Tp53/Uhrf1* DKO, along with the observation of three *Tp53/Rb1/Uhrf1* TKO mice with undetectable
303 tumors, suggested that early RB-pathway inactivation, and the associated UHRF1 overexpression, may
304 contribute to early stages of tumor promotion. To determine whether *Uhrf1* contributes to tumor
305 promotion or tumor progression, we performed periodic FDG-PET/microCT scans on *Tp53/Rb1* DKO and
306 *Tp53/Rb1/Uhrf1* TKO mice to determine the age at which tumors are detectable (Fig. 1I). In *Tp53/Rb1* DKO
307 mice, tumors were detected in average at 30.8 ± 2.9 weeks (n=4) while in *Tp53/Rb1/Uhrf1* TKO mice,
308 tumors were detected significantly later at 41.1 ± 6.6 weeks (n=4; p=0.0362; Fig. 1J). All test subjects
309 reached humane end-of-study within 3 weeks of first tumor detection. These data suggest that *Uhrf1*
310 plays a pivotal role in the early developmental process of OS tumor promotion following loss of *Rb1*.
311
312
313 **UHRF1 overexpression correlates with increased malignancy and metastasis in human OS**
314
315 Following the observation of UHRF1 contributing to a more aggressive phenotype in developmental
316 mouse models of OS, we next examined the role of UHRF1 in human OS. Upon examination of The Cancer
317 Genome Atlas (TCGA) database, we found that *UHRF1* is significantly overexpressed in malignancies that
318 frequently inactivate the RB-pathway including sarcomas, breast invasive carcinomas, and lung
319 adenocarcinomas; while tumors where RB loss is infrequent in primary disease, such as prostate
320 adenocarcinomas [26], show no significant difference in *UHRF1* compared to control normal tissue (Fig.

321 2A). Furthermore, in sarcomas, high *UHRF1* expression is associated with poorer survival (Fig. 2B). Since
322 OS is not represented in the TCGA sarcoma tumor cohort, we performed *in situ* hybridization of a human
323 OS tissue array to identify the presence of *UHRF1* mRNA in the 25 primary OS tumors examined (Fig. 2C).
324 We observed that tumors expressing high *UHRF1* mRNA levels were classified as stage II and none as stage
325 I OS (Fig. 2D), suggesting that UHRF1 expression increases in more aggressive tumors. However, the
326 limited number of stage III and stage IV samples available restricted our analysis of metastatic cases. Given
327 the interesting possibility of a role of UHRF1 in OS metastasis shown by our mouse models, we analyzed
328 *UHRF1* expression from a published RNA-Seq dataset of pretreatment biopsies from 53 high-grade OS
329 patients who did or did not develop metastasis within 5 years of initial diagnosis, compared to normal
330 mesenchymal stem cells (MSC), and osteoblasts [27]. *UHRF1* expression in MSCs (log2 median = 9.055)
331 was similar to osteoblasts (log2 median = 8.510; p=0.1495) and tumors from patients that did not develop
332 metastasis within 5 years from the time of biopsy (log 2 median = 9.055; p=0.1123). However, tumors
333 from patients who developed metastasis within 5 years from the time of biopsy expressed significantly
334 higher levels of *UHRF1* (log2 mean = 9.880; p = 0.0015; Fig. 2E).
335
336 The clinical data led us to examine UHRF1 mRNA and protein levels in 4 different human OS cell lines:
337 143B, SJSA-1, SaOS-2 (RB-null cell line), and U-2 OS, along with 5 patient-derived orthotopic xenografts
338 (PDX1-5). qPCR analysis of human OS cell lines and PDX showed a significant upregulation of *UHRF1* mRNA
339 levels in all samples except PDX2 when compared to human mesenchymal stem cells (MSC), independent
340 of whether they express RB protein or not (Fig. 2F-G and Supp. Fig. 3A). At the protein level, UHRF1 was
341 highly overexpressed across all analyzed OS subjects compared to MSC controls (Fig. 2H-I).
342
343
344 ***UHRF1* is a direct target of the RB/E2F signaling pathway in the osteogenic lineage**

345

346 A few studies have reported UHRF1 as a direct E2F1 transcriptional target [28, 29]. Following our
347 observations that UHRF1 is overexpressed in all OS samples analyzed, we aimed to confirm whether
348 UHRF1 is a direct E2F1 target in the osteogenic lineage. We performed chromatin immunoprecipitation
349 (ChIP) analysis in MSC and found E2F1 enrichment at the E2F1 consensus binding motifs located within
350 the UHRF1 promoter (Supp. Fig. 3B). To confirm E2F1 drives *UHRF1* transcription in OS cells, we knocked-
351 down E2F1 using shRNA which resulted in a modest decrease in UHRF1 protein levels in OS cell lines (Supp.
352 Fig. 3C). Similarly, knockdown of another activator E2F, E2F3, showed mild to no effect on UHRF1 protein
353 levels (Supp. Fig. 3D). However, knockdown of E2F1 in combination with E2F3, but not in combination
354 with E2F2, significantly decreased UHRF1 protein levels (Supp. Fig. 3F). To further verify that UHRF1
355 expression is transcriptionally regulated by the RB/E2F pathway, human OS cell lines were treated with
356 palbociclib. Palbociclib is a CDK4/6 inhibitor that results in blockade of RB hyperphosphorylation and
357 thereby, E2F transcriptional repression. qPCR analysis revealed significant decreases in *UHRF1* mRNA
358 levels upon palbociclib treatment, with the exception of the RB-null cell line, SaOS-2, which served as a
359 negative control (Supp. Fig. 3G). Palbociclib treatment also decreased UHRF1 protein levels in a dose-
360 dependent manner in RB-positive OS cells, as revealed by Western Blot analysis (Supp. Fig. 3H). In line
361 with these results, we also observed upregulation of *CDK4* and/or *CDK6* transcripts in RB-wildtype OS cell
362 lines and/or *INK4A* downregulation (Supp. Fig. 3I-J). SJSA-1 is known to have *CDK4* amplification and U2-
363 OS to have *INK4A* deletion. Together, these data confirm transcriptional regulation of *UHRF1* by the
364 RB/E2F pathway through direct transcriptional activation by activator E2Fs, E2F1 and E2F3.

365

366

367 **UHRF1 promotes human OS proliferation *in vitro* and *in vivo***

368

369 Emerging reports have linked UHRF1 overexpression in cancer with its ability to promote proliferation,
370 migration/invasion, or both [11, 30-35]. To study the role of UHRF1 overexpression in OS, we first used
371 shRNA to UHRF1-knockdown in OS cell lines; however, we observed that UHRF1 knockdown could be
372 sustained for more than two weeks, complicating data reproducibility over time (data not shown). To
373 overcome this challenge, we generated UHRF1 CRISPR knockouts (KO) and a non-targeting vector control
374 (VC). Clones (n=3) were selected for SJSA-1 and 143B, while the other cell lines remained as pools and
375 were analyzed within 2-3 weeks after being generated. Western blot analysis revealed successful UHRF1
376 KO in all four OS cell lines tested (Fig. 3A). Growth curve analyses from these cells showed that UHRF1 KO
377 cells have longer doubling times compared to VC OS cells (Fig. 3B). This decrease in proliferation potential
378 was further evidenced through clonogenic assays showing significant reductions in both the number and
379 the size of colonies in UHRF1 KO compared to VC cells (Fig. 3D). To directly assess cell proliferation, we
380 labelled actively proliferating UHRF1 KO and VC cells using EdU and found significantly fewer EdU-positive
381 UHRF1 KO cells compared to VC, suggesting a slower rate of active DNA synthesis; with the exception of
382 U-2 OS, albeit a trend of decreased incorporation was still observed (Fig. 3E-F).
383
384 To assess proliferative capacity *in vivo*, SJSA-1 UHRF1 KO and VC OS cells were injected subcutaneously
385 into immune-deficient mice at opposite flank regions. UHRF1 KO cells gave rise to significantly smaller
386 tumors (average size 0.49 ± 0.37 cm^3 and average weight 0.70 ± 0.69 g) when compared to VC (average
387 volume 1.23 ± 0.75 cm^3 (p=0.02, n=10); and average weight 1.62 ± 1.09 g (p=0.01, n=10)). To test the
388 therapeutic potential of targeting UHRF1 in established tumors, we utilized a doxycycline-inducible
389 system to drive the expression of CRISPR gRNA against UHRF1. Inducible UHRF1 KO (iKO) and VC (iVC) OS
390 cells were subcutaneously injected, and tumors allowed to establish for one week. CRISPR/Cas-9 gRNAs
391 were then induced using oral doxycycline (Fig. 3G). SJSA-1 tumor growth was significantly reduced in
392 UHRF1 iKO tumors (average tumor volume 0.356 ± 0.201 cm^3 and weight 0.46 ± 0.45 g) compared to iVC

393 tumors (1.455 ± 0.865 cm^3 (p=0.02, n=5); and 1.80 ± 1.11 g (p=0.01, n=5)) (Fig. 3H-I). Western blot analyses
394 confirmed reduced UHRF1 protein levels in UHRF1 iKO tumors (Fig. 3K). UHRF1 iKO tumors also presented
395 phenotypic features of less aggressive tumors, as seen by lessened vasculature and ulceration compared
396 to iVC tumors (Fig. 3J). Induction of a different UHRF1 sgRNA in SJSA-1 resulted in similar tumor size
397 reduction, as well as with other OS cell lines (Supp. Fig. 4 A-D). Taken together, both *in vitro* and *in vivo*
398 data suggest that UHRF1 is critical for OS cell proliferation.
399
400
401 **UHRF1 promotes human OS cell migration and invasion *in vitro* and *in vivo***
402
403 The high metastatic potential of OS is the main cause of mortality in patients. Given that our mouse
404 models indicated a possible involvement of UHRF1 in OS metastasis, we sought to evaluate the role of
405 UHRF1 in promoting cell migration, invasion, and metastasis. Scratch-wound assays were used to assess
406 the migratory potential of UHRF1 KO OS cell lines (Fig. 4A). We observed a significant decrease in the
407 distance migrated in UHRF1 KO compared to VC OS cells for all cell lines studied, with an average of 56.8
408 ± 2.3% reduction in migration across the three cell lines (Fig. 4B). In addition to decreased migratory
409 potential, Transwell invasion assays revealed a significant reduction in the number of UHRF1 KO OS cells
410 capable of mobilizing across Matrigel-coated inserts in all OS cell lines (Fig. 4C-D).
411
412 To test whether the reduced migratory and invasive capacities observed *in vitro* translate into less
413 metastatic potential *in vivo*, we injected SJSA-1 UHRF1 KO and VC cells into the tail vein of immune-
414 deficient mice and assessed the rate of lung colonization 3-weeks post injection. We found that the lungs
415 of mice injected with SJSA-1 UHRF1 KO cells had a reduced number of metastatic nodules and a
416 significantly reduced tumor nodule size when compared to the lungs of mice injected with VC cells (Fig.

417 4E-G). We also observed a significant decrease in the burden of lung metastases when we injected SJSA-
418 1 UHRF1 iKO into the tail-vein of mice fed with doxycycline, compared to iVC cells (Fig. 4H-J), as reflected
419 by the reduced number (Fig. 4I) and significant decrease in size (Fig. 4J) of metastatic nodules. This
420 suggests that targeting UHRF1 would be an effective strategy to reduce the burden of lung metastases
421 even when tumor cells have already undergone intravasation.
422
423 To determine whether UHRF1 plays an intrinsic role in cell migration, we performed gain-of-function
424 studies using MSCs, the normal progenitors of the osteogenic tissue. We generated a doxycycline-
425 inducible lentiviral vector system to drive non-toxic UHRF1 overexpression (pCW57-UHRF1; Fig. 5A) and
426 used the empty vector as control (pCW57-VC). Western blot analysis confirmed successful induction of
427 UHRF1 overexpression upon doxycycline treatment in transduced MSCs (Fig. 5B). We found that UHRF1
428 overexpression in MSCs significantly increased migratory potential as evidenced by the robust increase in
429 the distance migrated (Fig. 5C-D) and number of cells invaded across Matrigel-coated Transwell
430 membranes (Fig. 5E-F) upon doxycycline induction in pCW57-UHRF1 cells compared to pCW57-VC using
431 scratch-wound assay.
432
433 We utilized this pCW57-UHRF1 vector to rescue high UHRF1 expression in UHRF1 KO OS cells. Doxycycline
434 treatment for 24 h was able to restore UHRF1 protein levels back to wild-type levels (Supp. Fig. 4E). The
435 rescue of UHRF1 expression resulted in a significant increase in migration in all OS cell lines (Supp. Fig. 4F).
436 Taken together, this results support a role of UHRF1 in OS migration and invasion.
437
438
439 **UHRF1 increases exosome and *PLAU* expression resulting in enhanced cell migration and invasion**
440

441 UHRF1 is required for maintenance of DNA methylation during DNA replication through the recruitment
442 of DNMT1 [36]. However, UHRF1 ubiquitin ligase activity also targets DNMT1 for degradation, with some
443 studies reporting that UHRF1 overexpression results in decreased DNA methylation [37, 38]. To determine
444 the effects of UHRF1 loss on DNA methylation, chromatin structure, and transcription, we analyzed global
445 DNA methylation, chromatin accessibility, and transcriptome changes. We probed genomic DNA isolated
446 from UHRF1 KO and VC cell lines with an antibody against 5-methyl cytosine (5meC) to assess global DNA
447 methylation. We found genomic 5meC levels were decreased in UHRF1 KO compared to VC across all OS
448 cell lines examined (Supp. Fig. 5A). This reduction in global DNA methylation in OS UHRF1 KO cells
449 compared to VC was confirmed by representation bisulfite sequencing analysis of differentially
450 methylated regions across the genome of VC and UHRF1 KO OS cells, which showed most of the changes
451 occurring at non-coding regions of the genome (Supp. Fig. 5B). We also analyzed changes in the chromatin
452 landscape upon loss of UHRF1 using ATAC-seq in 143B, SJSA-1, and SaOS-2 UHRF1 KO compared to VC
453 (Supp. Fig. 5C). Despite the role of UHRF1 in heterochromatin maintenance and the decreased genomic
454 levels in DNA methylation, we identified only 16 chromatin regions with significant changes in chromatin
455 accessibility across these 3 biological replicates (Supp. Table 2). Within these changes, the majority were
456 consistent with the role of UHRF1 chromatin repression, with approximately 69% (11/16) resulting in
457 opening of chromatin upon UHRF1 loss.
458
459 In line with modest changes in DNA methylation and chromatin accessibility, gene expression analysis
460 using RNA-seq revealed that the gene expression profile from UHRF1 KO cell lines present minor variability
461 from VC cells, as portrayed by the principal component analysis (PCA) plot (Supp. Fig. 5D). We identified
462 only 272 differentially expressed genes (DEGs), with 191 upregulated and 81 downregulated genes in
463 UHRF1 KO compared to VC cells. Of particular interest, gene ontology (GO) analysis for biological
464 processes of the downregulated DEGs showed an enrichment of genes involved in regulation of cell

465 adhesion and migration (Fig. 6A). GO analysis of cellular components exposed the enrichment of genes
466 involved in extracellular vesicle formation and cell adhesion, consistent with the less migratory phenotype
467 of UHRF1 KO OS cells (Fig. 6B). We confirmed the changes in gene expression observed among top 13
468 genes involved in regulation of cell migration (Fig. 6C) through qPCR (Fig. 6D).
469
470 To examine whether UHRF1 affects migration and invasion through exosomes, we first tested the
471 differential effects of conditioned media (24 h) from VC and UHRF1 KO cells on OS cell migration. We
472 found that conditioned media from OS VC cells significantly increased autologous OS cell migration
473 compared to fresh media (Fig. 7A, blue bars). While conditioned media derived from OS UHRF1 KO cells
474 also increased cell migration compared to fresh media, the VC cell migration when exposed to UHRF1 KO
475 conditioned media was lower than VC conditioned media (Fig. 7A, red bars). Interestingly, UHRF1 KO cells
476 also displayed a robust increase in cell migration when exposed to VC conditioned media, but not when
477 exposed with autologous UHRF1 KO conditioned media (Fig. 7B). This suggests that UHRF1 loss decreases
478 the secretion of pro-migratory factors to the extracellular matrix that can serve as an autologous signal to
479 stimulate OS cell migration but does not affect the ability of the cells to respond to these extracellular
480 factors. We next blocked exosome biogenesis/release using GW4869 and endocytosis using
481 chlorpromazine (CPZ). We found that both GW4869 and CPZ significantly reduced the cell migration
482 induced by OS conditioned media (Fig. 4C). Taken together, this indicates that UHRF1 overexpression
483 contributes to the expression and secretion of exosomes which contribute, at least in part, to increased
484 OS cell migration.
485
486 Plasminogen activator, Urokinase (*PLAU*) was one of the genes identified through the transcriptome
487 analysis to be potentially involved in UHRF1-mediated cell migration. Urokinase plasminogen activator
488 protein (uPA) is associated with cell migration and a known cargo protein in osteosarcoma-secreted

489 exosomes [39]. Significant decrease in the levels of the *PLAU* transcript were observed in UHRF1 KO OS
490 cells (Fig. 6D), as well as the tumors they form subcutaneously in immune-deficient mice, with an average
491 2.2-fold decrease when compared to tumors formed from VC cells (p=0.038, Fig. 6E). Thus, we tested
492 whether treatment with uPA inhibitors could decrease migratory potential and invasiveness of OS cells.
493 Scratch-wound assays of amiloride-treated OS cell lines showed a significant decrease in migratory
494 potential, with an average of 40.3 ± 11.9% decrease across all OS cell lines examined (Fig. 7A). A significant
495 decrease of invasiveness, as determined by Transwell invasion assay, was also observed upon amiloride
496 treatment (Fig. 7B-C). This confirmed uPA as an important contributor of OS migratory potential. In line
497 with our observations associating UHRF1 with uPA levels, amiloride treatment was also able to inhibit
498 UHRF1-induced cell migration in MSCs (Fig. 7D-E). BC 11 hydrobromide, a selective uPA inhibitor, was used
499 to further verify the role of uPA in OS cell migration. A 23.2 ± 10.2% decrease in migration is seen across
500 OS cell lines upon treatment (Fig. 7F). Taken together, we established a positive correlation between
501 UHRF1 expression levels and migration/invasion potential in the osteogenic lineage, with uPA as the
502 potential conduit between the two.
503
504
505 **DISCUSSION**
506
507 Metastasis remains the most frequent fatal complication of OS. The lack of significant breakthroughs
508 beyond the scope of standard chemotherapeutics targeting highly proliferative underscores a pressing
509 clinical need for new therapeutic strategies for OS. For decades, genetic alterations at the *RB1* gene have
510 been associated with increased mortality, metastasis and poor response to chemotherapy in OS [6-10, 40,
511 41]. However, the precise mechanism through which this occurs remains to be elucidated to facilitate the
512 development of better therapeutic strategies. In this study, we identified *UHRF1* as a direct target of

513 RB/E2F pathway. UHRF1 overexpression is directly correlated with increased OS malignancy and
514 metastatic disease in humans. Specifically, UHRF1 facilitates OS cell proliferative, invasive, and metastatic
515 capacity. Furthermore, we found that the decrease in survival associated with loss-of-function mutations
516 at the *Rb1* gene is critically mediated through the overexpression of UHRF1.
517
518 Studies from retinoblastoma, a cancer initiated by biallelic inactivation of the *RB1* gene, defined a central
519 role of RB in epigenetic control and a key role of RB/E2F-regulated chromatin remodelers in tumorigenesis
520 [11, 42, 43]. Among these chromatin remodelers, UHRF1 was identified as a potential critical regulator of
521 tumor initiation and progression following RB-pathway deregulation that is overexpressed in several
522 cancers [11-15]. We confirmed *UHRF1* upregulation in human OS cell lines, PDXs, and primary OS tissue.
523 UHRF1 protein overexpression is recapitulated in both *p53* cKO and *Tp53*/*Rb1* DKO OS mouse model,
524 validating the suitability of this mouse model for the study of OS. Direct regulation of UHRF1 by the RB/E2F
525 signaling pathway was described previously, though in limited context [28, 29]. We established that
526 *UHRF1* expression is transcriptionally regulated by the RB/E2F signaling pathway in the osteogenic lineage.
527 ChIP analysis revealed enrichment of E2F1 at putative binding motifs within the promoter region of *UHRF1*.
528 However, E2F1 knockdown was insufficient in reducing UHRF1 expression. Rather, significant reduction
529 of UHRF1 level was achieved only through combined knockdown of E2F1 and E2F3, suggesting
530 compensatory mechanisms between activator E2Fs in regulating the transcription of downstream targets.
531 As the RB/E2F signaling pathway is often inactivated in cancer through mechanisms other than *RB1* loss-
532 of-function mutations, the most common being RB hyperphosphorylation through CDK4/6 activation or
533 p16 inactivation [17, 44, 45], it is not surprising that UHRF1 upregulation and overexpression in OS is not
534 restricted to *RB1*-null cases. UHRF1 overexpression in *RB1*-wildtype OS cell lines results from the
535 upregulation of *CDK4* and/or *CDK6*, which leads to RB hyperphosphorylation, preventing the repression

536 of E2F binding activities. This was confirmed by the down-regulation of *UHRF1* and dose-dependent
537 decrease of UHRF1 upon treatment with palbociclib, a known CDK4/6 inhibitor [46].
538
539 UHRF1 expression is positively correlated with cell proliferation and cell mobility in both normal and
540 malignant cells *in vitro* [11, 32-35]. Although it is clear that UHRF1 expression is linked to cellular
541 phenotypes that strongly associate with tumor malignancy, the link between UHRF1, OS tumor
542 progression, and its role in the poor prognosis associated with *RB1* loss has not been established. Our
543 results showed that UHRF1 KO decreases clonogenicity and tumor growth both *in vitro* and *in vivo*.
544 Independent from its role on proliferation, UHRF1 has a clear effect on the migratory potential of the
545 osteoblastic lineage as UHRF1 overexpression was sufficient to increase migration and invasion of normal
546 MSCs and targeting UHRF1 drastically reduced migration, invasion and metastatic capacity of OS cell lines.
547 It is important to note that although *RB1*-null status has been clinically associated with poor disease
548 outlook, the *RB1*-null cell line, SaOS-2, does not exhibit higher aggressiveness in comparison to other cell
549 lines. This could be explained by the limitation of utilizing cell lines, in which loss of clinical representation
550 is commonly seen. Our results also present a novel role of UHRF1 in the control of exosome formation
551 and suggest that uPA is critical for UHRF1-mediated migration. Exosomes and their cargo have been
552 implicated in osteosarcoma metastasis [47]. Here we show that UHRF1 can alter the expression of
553 exosomal components as well as their protein cargo composition. uPA is a serine protease that has long
554 been associated with tumor malignancy, being associated with cell migration and a known cargo protein
555 in osteosarcoma-secreted exosomes [39]. Upon conversion of plasminogen into plasmin, uPA triggers a
556 proteolytic cascade that leads to the degradation of extracellular matrix, an event necessary for
557 angiogenesis and metastasis. Our findings are in line with a previous study describing the uPA/uPAR axis
558 as a metastatic driver in OS [48]. While our results suggest that targeting UHRF1 might result in a more
559 robust therapeutic outcome, the observation that the UHRF1 induced cell migration can be reversed by

560 treatment with uPA inhibitors like amiloride [49] and BC11 hydrobromide, provides a therapeutic
561 alternative that can be further explored.
562
563 Our group is the first to model the critical role of UHRF1 in osteosarcomagenesis, with *Uhrf1* KO resulting
564 in a dramatic increase in overall survival and decrease in metastases, particularly in *Rb1*-null OS. Indeed,
565 median survival and rate of metastasis of *Tp53*/*Rb1*/*Uhrf1* TKO closely resembled that of *Tp53* cKO mice,
566 indicating that UHRF1 is a major driver of *Rb1* loss-associated malignancy. Interestingly, our results also
567 indicate that the increased survival in *Tp53*/*Rb1*/*Uhrf1* TKO mice is largely a result of delayed tumor
568 promotion, with negligible differences in tumor growth rates once the tumors have been detected. This
569 is quite distinct from our observations targeting UHRF1 in established tumor cells, suggesting there might
570 be compensatory pathways arising in the developmental tumor models. Further studies on tumors arising
571 from these developmental OS models might provide insight on potential compensatory mechanisms of
572 *Uhrf1* loss which may be relevant for predicting mechanisms of resistance for future UHRF1-targeted
573 therapeutics.
574
575 While targeting *Uhrf1* in developmental mouse models showed a distinct improvement in survival in *Rb1*-
576 null tumors over *Rb1*-wildtype, such distinctions were not observed in UHRF1 overexpressing human OS
577 cell lines. Both *RB1*-null and *RB1*-wildtype OS cell lines appear to equally benefit from targeting UHRF1. It
578 is possible that the timing of UHRF1 overexpression is crucial for the resulting poor prognosis. Early *Rb1*
579 loss would result in immediate UHRF1 overexpression which quickly promotes tumorigenesis compared
580 to tumors that eventually inactivate the RB/E2F pathway through alternative mechanisms. Supporting this
581 theory, *Tp53/Uhrf1* DKO mice showed some improvement in survival compared to the more aggressive
582 *Tp53* cKO mice that showed RB/E2F pathway inactivation. Alternatively, the RB/E2F complex is known not
583 only for its role in direct transcriptional repression, but also as epigenetic modifiers through the

584 recruitment of chromatin remodelers [42, 50-53]. Two UHRF1 domains, PHD and RING, contain LXCXE RB-
585 binding motifs [54]. Unpublished data from our group shows UHRF1 preferentially binds to
586 hyperphosphorylated RB. Thus, *RB1*-wildtype OS cells may preserve protein-protein interactions and RB
587 regulation on UHRF1. The possible loss of this layer of regulation in *RB1*-null tumors could account for the
588 drastic difference in clinical prognosis, supporting the view that the inactivation of RB by phosphorylation
589 is not functionally equivalent to the mutation of the *RB1* gene [55]. Further unpublished data from our
590 group strongly supports a critical role of UHRF1 in aiding RB-mediated tumorigenesis, with loss of *Uhrf1*
591 completely abrogating tumor formation in an *Rb1/p107* knockout model of retinoblastoma and
592 significantly increasing survival of a *Tp53/Rb1* model of small cell lung cancer, similar to the observations
593 presented for OS in this study.
594
595 In summary, this study provides evidence supporting UHRF1 targeting as a novel therapeutic strategy in
596 treating OS. We showed that UHRF1 targeting holds great potential in overcoming the highly metastatic
597 characteristic of OS, the main reason why survival rate has remained stagnant in past decades. We stand
598 to be the first to model the effect of UHRF1 throughout development and showed minimal on-target
599 toxicity, as opposed to various chemotherapeutic agents known to affect bone homeostasis [56].
600 Moreover, the degree to which UHRF1 loss reverted the increased malignancy upon *Rb1* loss suggests
601 that the benefit of UHRF1 targeting could go beyond the scope of OS by improving current treatment
602 paradigms of other cancers harboring RB/E2F pathway inactivation.
603
604
605 **ACKNOWLEDGEMENTS**
606 We thank Erin Yamanaka, Josselyn Peña, Sara Akhlaghi, and Annie Jeon for help with mouse genotyping
607 and cell culture; Christopher Liang for help with FDG-PET/microCT scans; Dr. Ali Nael, Dr. Robert Edwards

608 and Dr. Aaron Sassoon for assistance with pathology analysis. This work was supported in part by grants
609 to C.A.B. from the NIH (CA178207 and CA229696), the American Cancer Society (129801-IRG-16-187-13
610 and 133403-RSG-19-031-01-DMC) and the 2018 AACR-Aflac, Inc. Career Development Award for Pediatric
611 Cancer Research (18-20-10-BENA). J.L. and K.S. were supported by the NIH-MARC U-STAR training grant
612 (T34GM136498). This work was also made possible, in part, through access to the Genomics High
613 Throughput Facility Shared Resource of the Cancer Center Support Grant (P30CA-062203) at the
614 University of California, Irvine and NIH shared instrumentation grants 1S10RR025496-01, 1S10OD010794-
615 01, and 1S10OD021718-01.

616

617 *Author contributions:* C.A.B. conceived the project. S.C.W., A.K., L.Z., J.L., K.S., and C.A.B. performed the
618 experiments. J.W. and C.C. performed the sequencing data analysis. S.W. and C.A.B. wrote the manuscript.

619 **References**

620 1. Ottaviani, G. and N. Jaffe, *The epidemiology of osteosarcoma.* Cancer treatment and research,
621 2009. **152**: p. 3-13.
622 2. Huang, Y.M., et al., *The metastasectomy and timing of pulmonary metastases on the outcome of*
623 *osteosarcoma patients.* Clin Med Oncol, 2009. **3**: p. 99-105.
624 3. Mirabello, L., R.J. Troisi, and S.A. Savage, *Osteosarcoma Incidence and Survival Rates From 1973*
625 *to 2004 Data From the Surveillance, Epidemiology, and End Results Program.* Cancer, 2009.
626 **115**(7): p. 1531-1543.
627 4. Martin, J.W., J.A. Squire, and M. Zielenska, *The genetics of osteosarcoma.* Sarcoma, 2012. **2012**:
628 p. 627254.
629 5. Chen, X., et al., *Recurrent somatic structural variations contribute to tumorigenesis in pediatric*
630 *osteosarcoma.* Cell Rep, 2014. **7**(1): p. 104-12.
631 6. Feugeas, O., et al., *Loss of heterozygosity of the RB gene is a poor prognostic factor in patients*
632 *with osteosarcoma.* J Clin Oncol, 1996. **14**(2): p. 467-72.
633 7. Benassi, M.S., et al., *Altered G1 phase regulation in osteosarcoma.* Int J Cancer, 1997. **74**(5): p.
634 518-22.
635 8. Goto, A., et al., *Association of loss of heterozygosity at the p53 locus with chemoresistance in*
636 *osteosarcomas.* Jpn J Cancer Res, 1998. **89**(5): p. 539-47.
637 9. Wadayama, B., et al., *Mutation spectrum of the retinoblastoma gene in osteosarcomas.* Cancer
638 Res, 1994. **54**(11): p. 3042-8.
639 10. Ren, W. and G. Gu, *Prognostic implications of RB1 tumour suppressor gene alterations in the*
640 *clinical outcome of human osteosarcoma: a meta-analysis.* Eur J Cancer Care (Engl), 2017. **26**(1).
641 11. Benavente, C.A., et al., *Chromatin remodelers HELLS and UHRF1 mediate the epigenetic*
642 *deregulation of genes that drive retinoblastoma tumor progression.* Oncotarget, 2014. **5**(20): p.
643 9594-9608.
644 12. Mousli, M., et al., *ICBP90 belongs to a new family of proteins with an expression that is*
645 *deregulated in cancer cells.* British journal of cancer, 2003. **89**(1): p. 120-7.
646 13. Unoki, M., et al., *UHRF1 is a novel molecular marker for diagnosis and the prognosis of bladder*
647 *cancer.* Br J Cancer, 2009. **101**(1): p. 98-105.
648 14. Daskalos, A., et al., *UHRF1-mediated tumor suppressor gene inactivation in nonsmall cell lung*
649 *cancer.* Cancer, 2011. **117**(5): p. 1027-37.
650 15. Kofunato, Y., et al., *UHRF1 expression is upregulated and associated with cellular proliferation in*
651 *colorectal cancer.* Oncol Rep, 2012. **28**(6): p. 1997-2002.
652 16. Stewart, E., et al., *The Childhood Solid Tumor Network: A new resource for the developmental*
653 *biology and oncology research communities.* Dev Biol, 2016. **411**(2): p. 287-293.
654 17. Wu, S.C. and C.A. Benavente, *Chromatin remodeling protein HELLS is upregulated by inactivation*
655 *of the RB-E2F pathway and is nonessential for osteosarcoma tumorigenesis.* Oncotarget, 2018.
656 **9**(66): p. 32580-32592.
657 18. Benavente, C.A., et al., *Cross-species genomic and epigenomic landscape of retinoblastoma.*
658 Oncotarget, 2013. **4**(6): p. 844-59.
659 19. Dobin, A., et al., *STAR: ultrafast universal RNA-seq aligner.* Bioinformatics, 2013. **29**(1): p. 15-21.
660 20. Anders, S., P.T. Pyl, and W. Huber, *HTSeq--a Python framework to work with high-throughput*
661 *sequencing data.* Bioinformatics, 2015. **31**(2): p. 166-9.
662 21. Love, M.I., W. Huber, and S. Anders, *Moderated estimation of fold change and dispersion for*
663 *RNA-seq data with DESeq2.* Genome Biol, 2014. **15**(12): p. 550.
664 22. Edgar, R., M. Domrachev, and A.E. Lash, *Gene Expression Omnibus: NCBI gene expression and*
665 *hybridization array data repository.* Nucleic Acids Res, 2002. **30**(1): p. 207-10.

666 23. Walkley, C.R., et al., *Conditional mouse osteosarcoma, dependent on p53 loss and potentiated by*
667 *loss of Rb, mimics the human disease.* Genes Dev, 2008. **22**(12): p. 1662-76.
668 24. Berman, S.D., et al., *Metastatic osteosarcoma induced by inactivation of Rb and p53 in the*
669 *osteoblast lineage.* Proceedings of the National Academy of Sciences of the United States of
670 America, 2008. **105**(33): p. 11851-6.
671 25. Muto, M., et al., *Targeted disruption of Np95 gene renders murine embryonic stem cells*
672 *hypersensitive to DNA damaging agents and DNA replication blocks.* J Biol Chem, 2002. **277**(37):
673 p. 34549-55.
674 26. Aparicio, A., R.B. Den, and K.E. Knudsen, *Time to stratify? The retinoblastoma protein in*
675 *castrate-resistant prostate cancer.* Nat Rev Urol, 2011. **8**(10): p. 562-8.
676 27. Kuijjer, M.L., et al., *Identification of osteosarcoma driver genes by integrative analysis of copy*
677 *number and gene expression data.* Genes Chromosomes Cancer, 2012. **51**(7): p. 696-706.
678 28. Magri, L., et al., *E2F1 coregulates cell cycle genes and chromatin components during the*
679 *transition of oligodendrocyte progenitors from proliferation to differentiation.* The Journal of
680 neuroscience : the official journal of the Society for Neuroscience, 2014. **34**(4): p. 1481-93.
681 29. Unoki, M., T. Nishidate, and Y. Nakamura, *ICBP90, an E2F-1 target, recruits HDAC1 and binds to*
682 *methyl-CpG through its SRA domain.* Oncogene, 2004. **23**(46): p. 7601-10.
683 30. Guan, D., et al., *The epigenetic regulator UHRF1 promotes ubiquitination-mediated degradation*
684 *of the tumor-suppressor protein promyelocytic leukemia protein.* Oncogene, 2013. **32**(33): p.
685 3819-3828.
686 31. Zhang, Y., et al., *Upregulated UHRF1 Promotes Bladder Cancer Cell Invasion by Epigenetic*
687 *Silencing of KiSS1.* PLoS One, 2014. **9**(10): p. Article No.: e104252.
688 32. Zhang, Z.-Y., et al., *Clinicopathological analysis of UHRF1 expression in medulloblastoma tissues*
689 *and its regulation on tumor cell proliferation.* Medical Oncology (Totowa), 2016. **33**(9): p. Article
690 No.: 99.
691 33. Zhu, M., et al., *Regulation of UHRF1 by microRNA-9 modulates colorectal cancer cell*
692 *proliferation and apoptosis.* Cancer Science, 2015. **106**(7): p. 833-839.
693 34. Cui, L., et al., *Up-regulation of UHRF1 by oncogenic Ras promoted the growth, migration, and*
694 *metastasis of pancreatic cancer cells.* Molecular and Cellular Biochemistry, 2015. **400**(1-2): p.
695 223-232.
696 35. Li, X.-L., et al., *Exogenous expression of UHRF1 promotes proliferation and metastasis of breast*
697 *cancer cells.* Oncology Reports, 2012. **28**(1): p. 375-383.
698 36. Bostick, M., et al., *UHRF1 plays a role in maintaining DNA methylation in mammalian cells.*
699 Science, 2007. **317**(5845): p. 1760-4.
700 37. Du, Z., et al., *DNMT1 stability is regulated by proteins coordinating deubiquitination and*
701 *acetylation-driven ubiquitination.* Sci Signal, 2010. **3**(146): p. ra80.
702 38. Mudbhary, R., et al., *UHRF1 overexpression drives DNA hypomethylation and hepatocellular*
703 *carcinoma.* Cancer Cell, 2014. **25**(2): p. 196-209.
704 39. Endo-Munoz, L., et al., *Progression of Osteosarcoma from a Non-Metastatic to a Metastatic*
705 *Phenotype Is Causally Associated with Activation of an Autocrine and Paracrine uPA Axis.* Plos
706 One, 2015. **10**(8).
707 40. Benassi, M.S., et al., *Alteration of pRb/p16/cdk4 regulation in human osteosarcoma.* Int J Cancer,
708 1999. **84**(5): p. 489-93.
709 41. Maitra, A., et al., *Loss of p16(INK4a) expression correlates with decreased survival in pediatric*
710 *osteosarcomas.* Int J Cancer, 2001. **95**(1): p. 34-8.
711 42. Zhang, J., et al., *A novel retinoblastoma therapy from genomic and epigenetic analyses.* Nature,
712 2012. **481**(7381): p. 329-34.

713 43. Benavente, C.A. and M.A. Dyer, *Genetics and epigenetics of human retinoblastoma.* Annu Rev
714 Pathol, 2015. **10**: p. 547-62.
715 44. Rane, S.G., et al., *Germ line transmission of the Cdk4(R24C) mutation facilitates tumorigenesis*
716 *and escape from cellular senescence.* Mol Cell Biol, 2002. **22**(2): p. 644-56.
717 45. Nuovo, G.J., et al., *In situ detection of the hypermethylation-induced inactivation of the p16 gene*
718 *as an early event in oncogenesis.* Proc Natl Acad Sci U S A, 1999. **96**(22): p. 12754-9.
719 46. Fry, D.W., et al., *Specific inhibition of cyclin-dependent kinase 4/6 by PD 0332991 and associated*
720 *antitumor activity in human tumor xenografts.* Mol Cancer Ther, 2004. **3**(11): p. 1427-38.
721 47. Jerez, S., et al., *Extracellular vesicles from osteosarcoma cell lines contain miRNAs associated*
722 *with cell adhesion and apoptosis.* Gene, 2019. **710**: p. 246-257.
723 48. Endo-Munoz, L., et al., *Progression of Osteosarcoma from a Non-Metastatic to a Metastatic*
724 *Phenotype Is Causally Associated with Activation of an Autocrine and Paracrine uPA Axis.* PLoS
725 One, 2015. **10**(8): p. e0133592.
726 49. Vassalli, J.D. and D. Belin, *Amiloride selectively inhibits the urokinase-type plasminogen*
727 *activator.* FEBS Lett, 1987. **214**(1): p. 187-91.
728 50. Chi, P., C.D. Allis, and G.G. Wang, *Covalent histone modifications--miswritten, misinterpreted and*
729 *mis-erased in human cancers.* Nat Rev Cancer. **10**(7): p. 457-69.
730 51. Lu, J., et al., *A genome-wide RNA interference screen identifies putative chromatin regulators*
731 *essential for E2F repression.* Proc Natl Acad Sci U S A, 2007. **104**(22): p. 9381-6.
732 52. Benetti, R., et al., *A mammalian microRNA cluster controls DNA methylation and telomere*
733 *recombination via Rbl2-dependent regulation of DNA methyltransferases.* Nat Struct Mol Biol,
734 2008. **15**(9): p. 998.
735 53. Wen, H., et al., *Epigenetic regulation of gene expression by Drosophila Myb and E2F2-RBF via the*
736 *Myb-MuvB/dREAM complex.* Genes Dev, 2008. **22**(5): p. 601-14.
737 54. Jeanblanc, M., et al., *The retinoblastoma gene and its product are targeted by ICBP90: a key*
738 *mechanism in the G1/S transition during the cell cycle.* Oncogene, 2005. **24**(49): p. 7337-7345.
739 55. Dyson, N.J., *RB1: a prototype tumor suppressor and an enigma.* Genes Dev, 2016. **30**(13): p.
740 1492-502.
741 56. Madan, B., et al., *Bone loss from Wnt inhibition mitigated by concurrent alendronate therapy.*
742 Bone Res, 2018. **6**: p. 17.

743

744

Wu et al
Figure 1

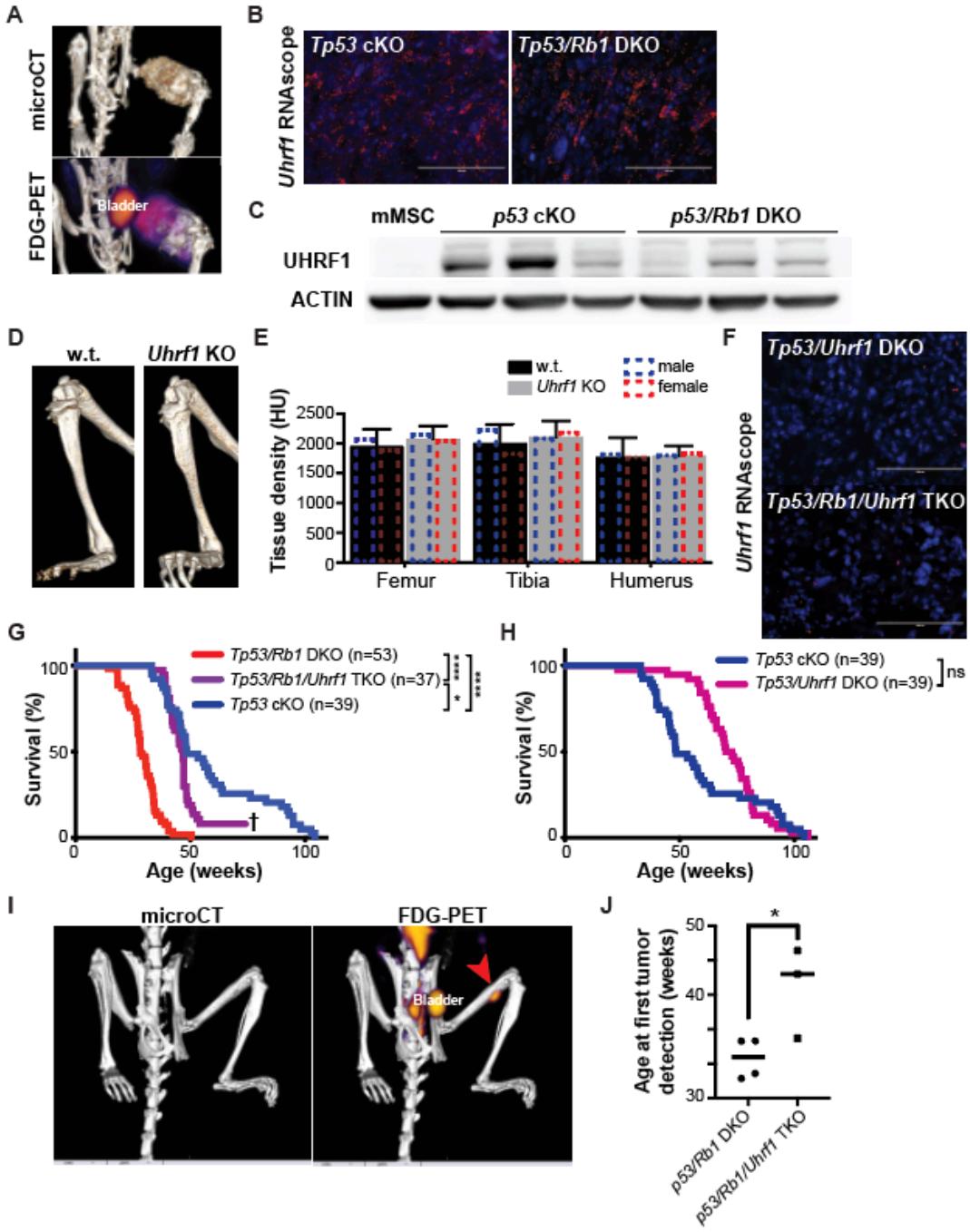

745

746 **Figure 1. UHRF1 is a critical driver of the increased malignancy observed in *Rb1* null OS**

747 (A) Representative micro-CT (top) and micro-PET (bottom) scans of OS that arises in a mouse femur. (B)

748 Representative fluorescent images of *in situ* hybridizations using RNAscope on tumors from genetically

749 engineered OS mice using a probe against *Uhrf1* (red). Nuclei were counterstained with DAPI (blue). *Uhrf1*
750 expression is detected in *Tp53* cKO and *Tp53/Rb1* DKO mice. (C) Western blot detection of UHRF1 in
751 tumors from genetically engineered *p53* cKO and *p53/Rb1* DKO OS mice, β-actin was used as loading
752 control. (D) Micro-CT scan of hind limb from wildtype (w.t.) and preosteoblastic *Uhrf1* knockout (*Uhrf1*
753 KO) mice (E) Bone density analysis of prime OS locations in Hounsfield units (HU). Each data point is mean
754 ± s.d. of n=4 samples. (F) Representative fluorescent images of *in situ* hybridizations using RNAscope on
755 tumors from genetically engineered OS mice using a probe against *Uhrf1* (red). Nuclei were
756 counterstained with DAPI (blue). *Uhrf1* expression is not detected in *Tp53/Uhrf1* DKO and
757 *Tp53/Rb1/Uhrf1* TKO mice. (G-H) Kaplan-Meier curves showing the survival of OS-prone mouse models.
758 (G) Mice bearing *Rb1* mutations *Tp53/Rb1* DKO: *Osx-Cre; p53*$^{lox/lox}$*; Rb1*$^{lox/lox}$ (red; n=53) have significantly
759 shorter lifespan compared to *Tp53* cKO: *Osx-Cre; p53*$^{lox/lox}$*; Rb1*$^{lox/lox}$ (blue; n=39). This survival time was
760 significantly increased in *Tp53*/*Rb1*/*Uhrf1* TKO: *Osx-Cre; p53*$^{lox/lox}$*; Rb1*$^{lox/lox}$;*Uhrf1*$^{lox/lox}$ (purple; n=37) mice.
761 † Three surviving mice were removed from study to confirm tumor absence. (H) *Tp53*/*Uhrf1* DKO: *Osx-*
762 *Cre; p53*$^{lox/lox}$*; Uhrf1*$^{lox/lox}$ (magenta; n=39) showed an overall survival comparable to *Tp53* cKO (blue; n=39).
763 Mantel-Cox test were used for curve comparisons. ns=not significant, * $p < 0.05$, **** $p < 0.0001$. (I)
764 Representative images from micro-CT (left) and micro-PET (right) scans used for determining the age at
765 which tumors can be first detected (red arrow). (J) Age of mice (in weeks) at earliest tumor detection via
766 micro-CT and PET scans. Solid line represents the average for *Tp53/Rb1* DKO (n=4) and *Tp53*/*Rb1*/*Uhrf1*
767 TKO (n=3). *$p < 0.05$ by unpaired two-tailed *t* test.
768

Wu et al
Figure 2

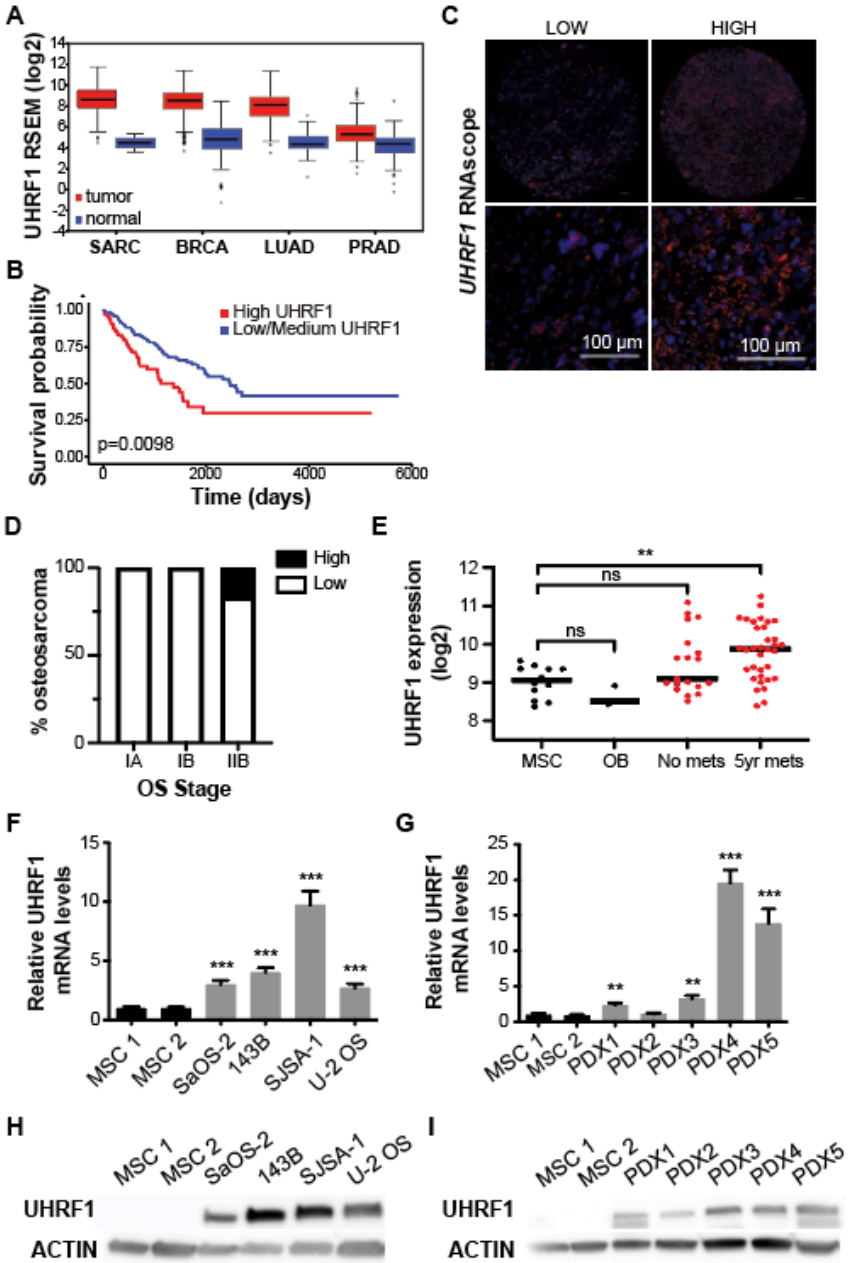

Figure 2. UHRF1 is upregulated and overexpressed in human OS

(A-B) The Cancer Genome Atlas data of (A) RNA-Seq by expectation-maximization (RSEM) values from 263 human sarcoma (SARC) tumor samples compared to 2 normal tissue (17.9-fold), 1100 breast invasive carcinoma (BRCA) compared to 112 normal (13.5-fold), 517 lung adenocarcinoma (LUAD) compared to 59 normal (13.7-fold) show increased *UHRF1* expression in tumors with frequent RB pathway alterations but

775 not in 498 prostate adenocarcinoma (PRAD) tumors compared 52 normal (1.84-fold) were RB pathway is
776 normally unaltered. Tumor samples (red) compared to normal samples (blue). (B) Effect of *UHRF1*
777 expression level on SARC patient survival comparing high UHRF1 expression (red; n=65) to low/medium
778 UHRF1 expression (blue; n=194). (C) Representative fluorescent images in 2X (top) and 20X (bottom)
779 magnification of *in situ* hybridizations using RNAscope scored as low or high based on signal intensity for
780 *UHRF1* mRNA. Scale bar = 100 µm. (D) Quantification of the percentage of low and high signal score
781 acquired from RNAscope in stage IA, IB, and IIB OS. (E) RNA-seq analysis comparing *UHRF1* expression
782 between mesenchymal stem cells (MSC), osteoblasts (OB), and high-grade OS biopsies from patients who
783 did (5yr mets) or did not develop metastasis (No mets) within 5 years from diagnoses showing increased
784 *UHRF1* expression in metastasis-prone tumors. (F-G) qPCR analysis of *UHRF1* mRNA in (F) human OS cell
785 lines (143B, SJSA-1, SaOS-2 and U-2 OS) and (G) patient-derived xenografts (PDX1-5). All data are mean ±
786 SD normalized to MSC (n=3). (H-I) Western blot detection of UHRF1 in (H) human OS cell lines, and (I) PDXs
787 tumors, β-actin was used as loading control. ** $p < 0.01$, *** $p < 0.001$ by unpaired two-tailed *t* test.

788

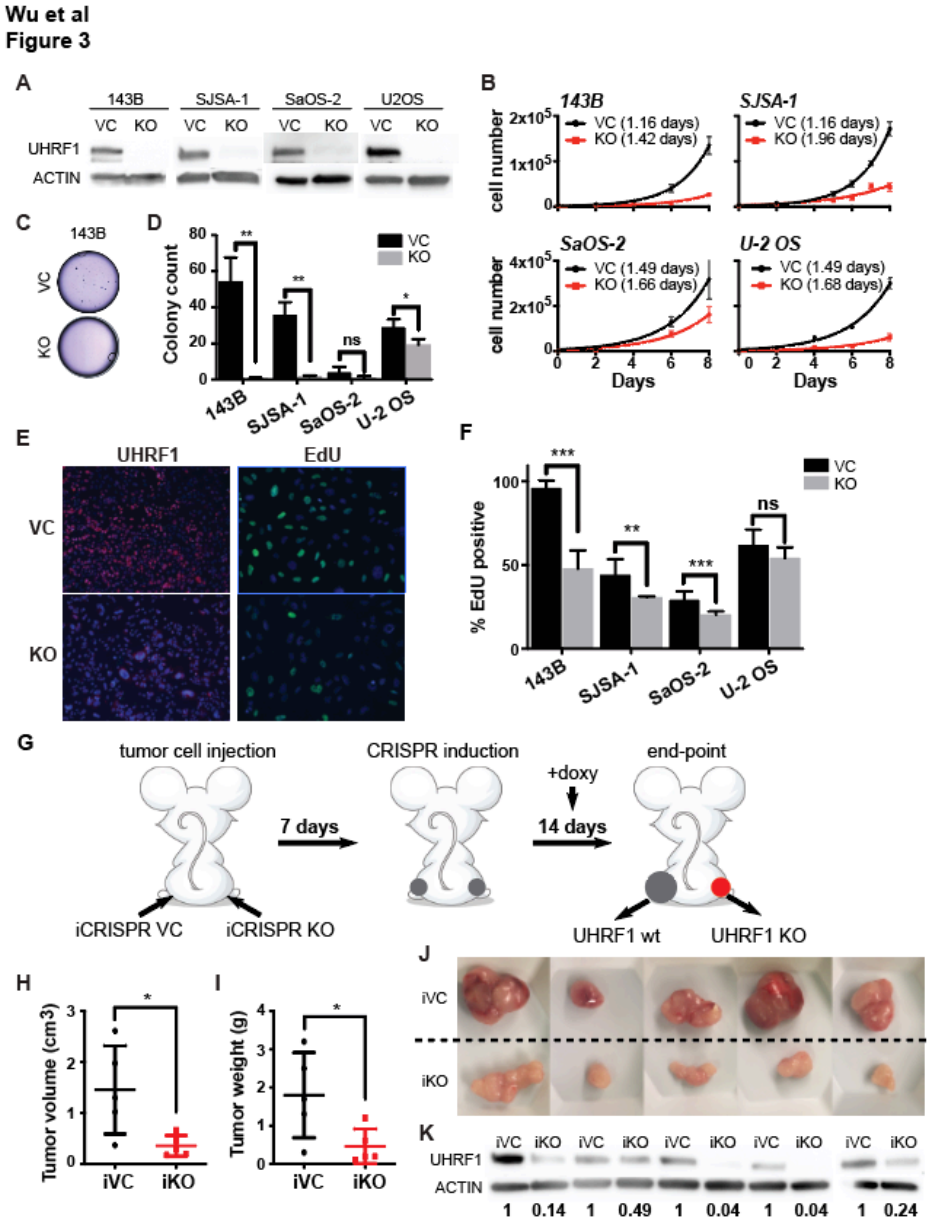

Figure 3. UHRF1 promotes human OS tumor growth *in vitro* and *in vivo*

(A) Western blot verification of CRISPR/Cas9-mediated UHRF1 knockout of human OS cell lines (KO) in comparison to non-targeting vector control (VC). β-actin was used as loading control. (B) Growth curves of UHRF1 knockout cells (KO, red) compared to control (VC, black), population doubling time indicated in parentheses. (C) Representative images from clonogenic assay plates with 143B VC and UHRF1 KO. (D) Histogram of colony counts from clonogenic assay. ns=not significant; * $p < 0.05$, ** $p < 0.01$ by unpaired two-tailed *t* test. (E) Representative images of cells labelled with Click-iT EdU (green) or immunostained

797 with UHRF1 (red). Nuclei were counterstained with DAPI (blue). (F) Quantification of EdU signal from
798 immunocytochemistry probing UHRF1 and EdU in VC and UHRF1 KO human OS cell lines. ns=not
799 significant; ** $p < 0.01$, *** $p < 0.001$ by unpaired two-tailed *t* test. (G) Cartoon representation for
800 doxycycline-inducible *in vivo* knockout for flank-injected OS cell lines carrying a non-targeting sgRNA
801 (iCRISPR VC) or UHRF1 sgRNA (iCRISPR KO). (H-I) Quantification of the tumor (H) volume and (I) weight for
802 each of the replicates. * $p<0.05$ by paired two-tailed *t* test. (J) Images from tumors collected from
803 subcutaneous injection of iCRISPR VC (iVC, n=5) and iCRISPR KO (iKO, n=5) SJSA-1. (K) Western blot
804 verification of UHRF1 knockout in iKO compared to iVC for tumors shown in J. β-actin was used as loading
805 control. UHRF1 densitometry quantification normalized to the matching iVC, prior normalization to β-
806 actin.
807

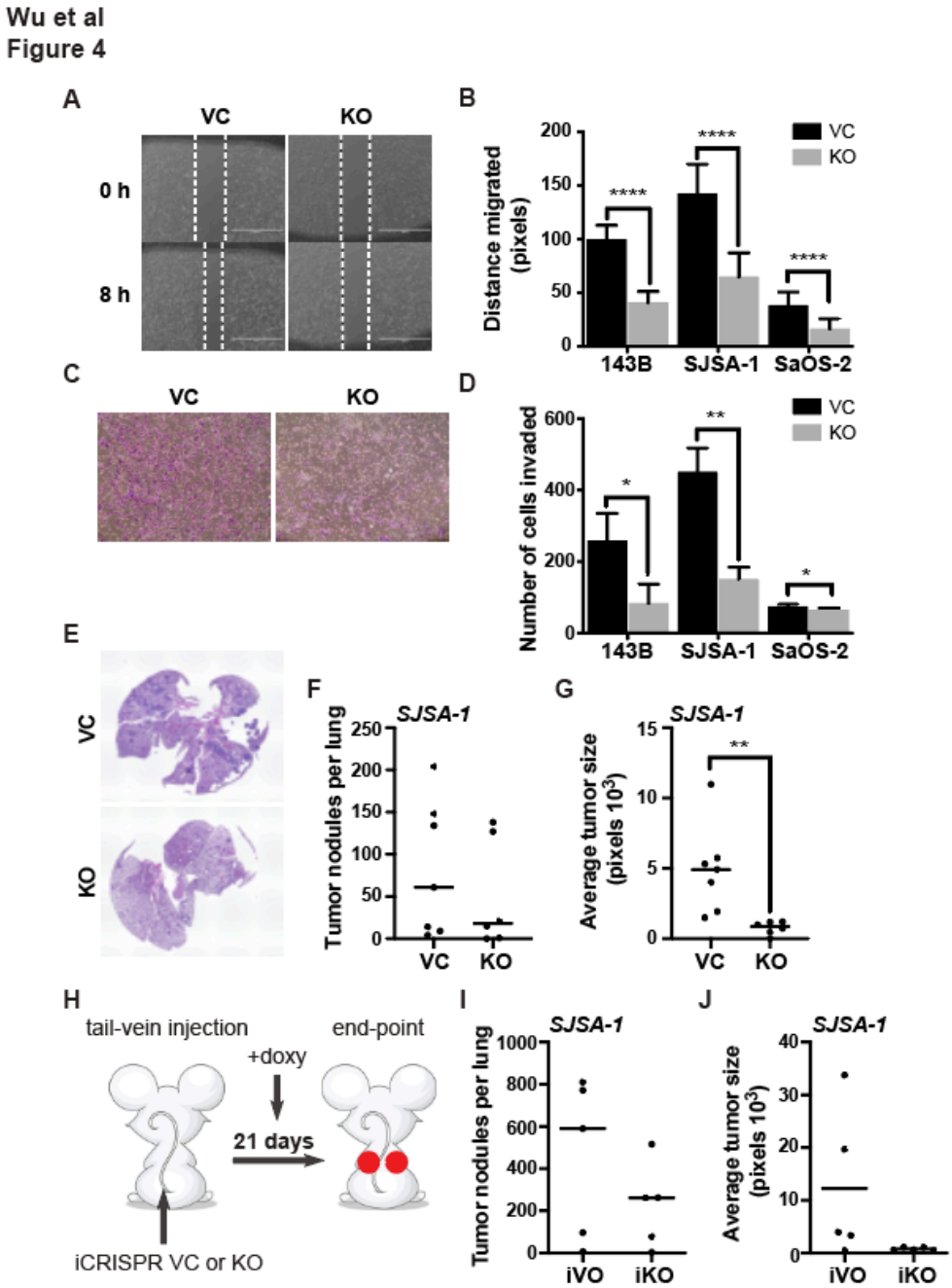

Figure 4. UHRF1 promotes human OS cell migration and invasion *in vitro* and *in vivo*

(A) Representative image from scratch-wound assay comparing wound closure of non-targeting vector control (VC) and UHRF1 KO (KO) cells over 8 h in SJSA-1 cells. White dashed lines represent wound edge. (B) Quantification of distance (pixels) migrated in scratch-wound assays for each of the OS cell lines. Each data point is mean ± s.d. of ten measurements in triplicate samples. (C) Representative images from

814 Transwell assays with cells stained with crystal violet (purple) comparing levels of invasion between VC
815 and UHRF1 KO in SJSA-1 cells. (D) Quantification of number of cells invaded across the Transwell
816 membrane for each of the OS cell lines. Each data point is mean ± s.d. of triplicate samples. (E)
817 Representative H&E staining from lung sections collected from mice injected intravenously with VC or
818 UHRF1 KO SJSA-1 cells. Pulmonary nodules were quantified by (F) the number of tumor nodules found per
819 lung and by (G) the average tumor size per lung. Solid line represents the average from n=7 for VC and
820 n=6 for KO. (H) Cartoon representation for doxycycline-inducible *in vivo* knockout for tail-vein-injected OS
821 cell lines carrying a non-targeting sgRNA (iCRISPR VC; iVC) or UHRF1 sgRNA (iCRISPR KO; iKO) to assess
822 lung metastases. (I-J) Pulmonary nodules were quantified by (I) the number of tumor nodules found per
823 lung and by (J) the average tumor size per lung. Solid line represents the average from five replicates for
824 each condition. For all graphs: ** $p < 0.01$, *** $p < 0.001$, **** $p < 0.0001$ by unpaired two-tailed *t* test.

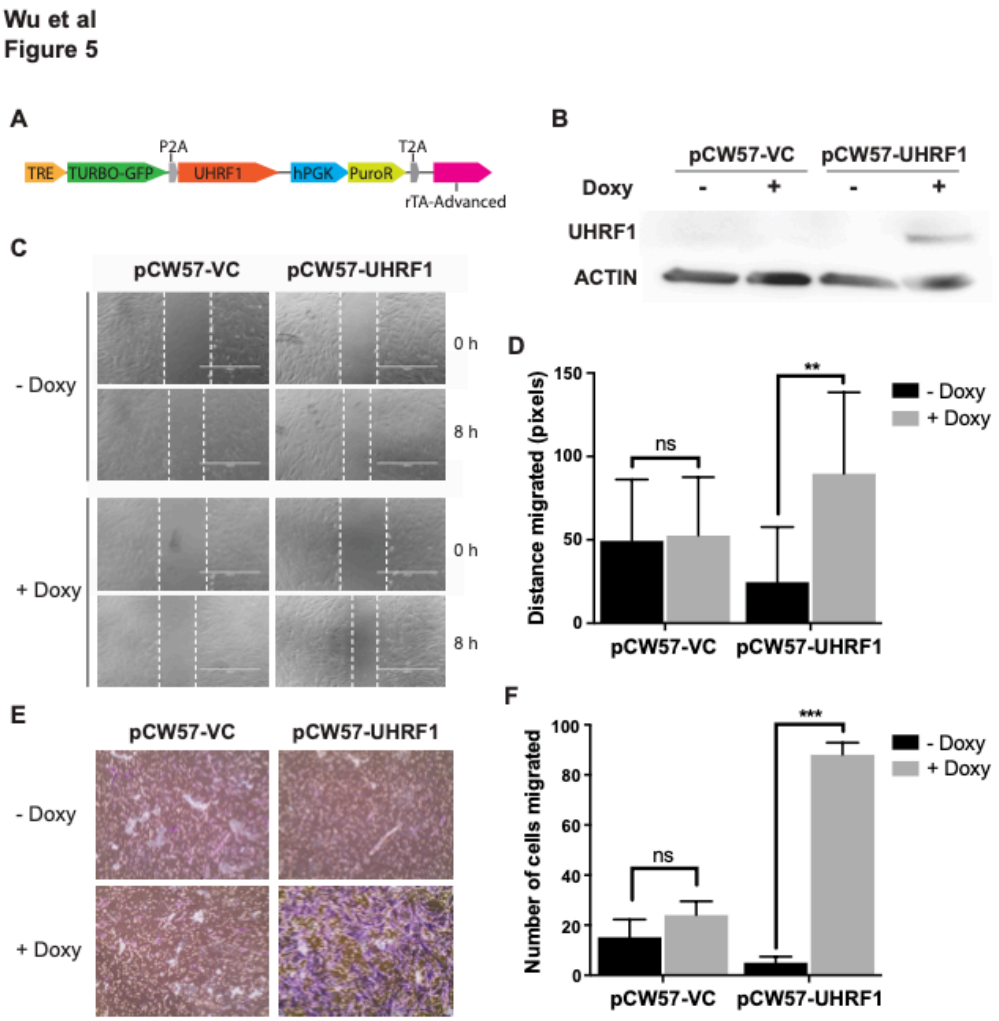

Figure 5. UHRF1 overexpression promotes human MSC cell migration and invasion

(A) Plasmid map of the doxycycline inducible UHRF1 overexpression system. Tet Response Element (TRE) is activated by doxycycline binding to the reverse tetracycline-controlled transactivator (rTA), allowing transcription of GFP and the pCW57-promoter driven human UHRF1 cDNA. (B) Western blot detection of UHRF1 in MSCs transduced with vector control (pCW57-VC) or UHRF1 overexpression (pCW57-UHRF1) plasmid, treated with DMSO (-) or doxycycline (+). (C) Scratch-wound assay in MSC culture comparing wound closure of control (pCW57-VC) and UHRF1 overexpressed (pCW57-UHRF1) cells over 8 h span. White dashed lines represent wound edge. (D) Histogram quantification of distance (pixels) migrated for doxycycline non-induced (black) and induced (gray) pCW57-VC and pCW57-UHRF1. Each data point is

835 mean ± s.d. of ten measurements in triplicate samples. (E) Representative images from Transwell assays
836 with cells stained with crystal violet comparing levels of invasion between doxycycline non-induced and
837 induced pCW57-VC and pCW57-UHRF1 MSC. (F) Quantification of the number of cells invaded across the
838 Transwell membrane. Each data point is mean ± s.d. of triplicate samples. For all graphs: ns=not significant,
839 ** $p < 0.01$, *** $p < 0.001$, by unpaired two-tailed *t* test.

Wu et al
Figure 6

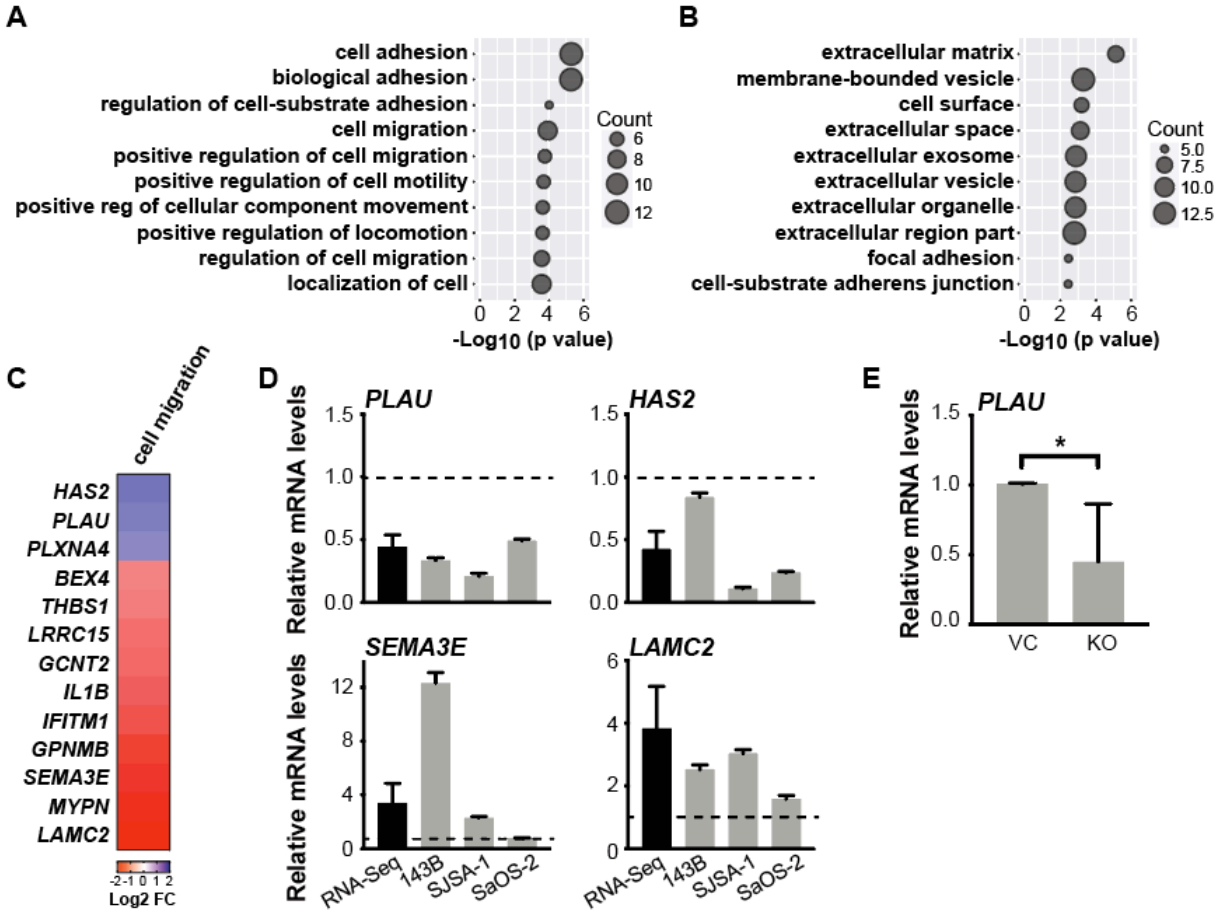

Figure 6. UHRF1 controls the expression of genes involved in exosomes and cell migration and invasion

(A) Gene ontology (GO) analysis for biological processes and (B) cellular components of the downregulated differentially expressed genes (DEGs) identified through RNA-seq. (C) Heat map of top 13 genes involved in regulation of cell migration, decreased (blue) or increased (red) in expression level upon UHRF1 loss. (D) qPCR analysis confirming expression changes of migration related genes in individual cell lines upon UHRF1 loss, fold change of mRNA level normalized to vector control (gray), compared with average fold change from RNA-seq analysis (black). (E) qPCR analysis of *PLAU* mRNA levels in flank-implanted tumors from control (VC) and UHRF1 KO (KO) SJSA-1 cell lines. * $p<0.05$ by paired two-tailed *t* test.

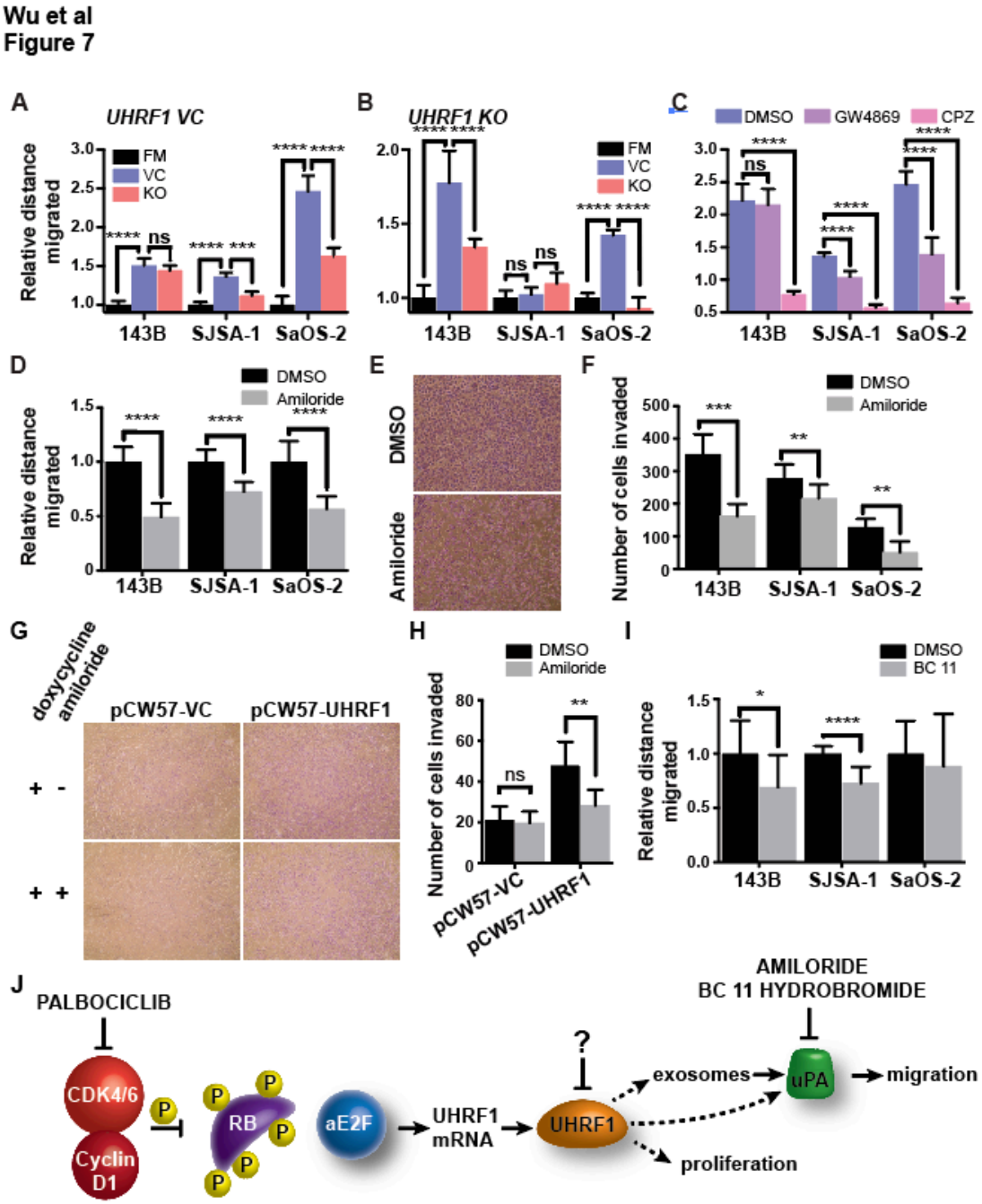

Figure 7. Exosome release and urokinase plasminogen activator contribute to OS migration

(A-D) Quantification of relative distance migrated in scratch-wound assays for (A) OS VC cells assayed with fresh media (FM) or conditioned media from VC cells or UHRF1 KO cells, normalized to FM; (B) OS UHRF1 KO cells assayed with FM or conditioned media from VC cells or UHRF1 KO cells, normalized to FM; (C) each of the OS cell lines treated with DMSO, 10 µM GW4869 or 20 µM CPZ, normalized to DMSO control;

855 (D) each of the OS cell lines treated with DMSO or 150 µM amiloride, normalized to DMSO control. Each
856 data point is mean ± s.d. of ten measurements in triplicate samples. (E) Representative images from
857 Transwell assays with cells stained with crystal violet comparing levels of invasion between cells treated
858 with DMSO or 150 µM amiloride in SJSA-1. (F) Quantification of the number of cells invaded in Transwell
859 invasion assay for each of the OS cell lines treated with DMSO or 150 µM amiloride. Each data point is
860 mean ± s.d. of triplicate samples. (G) Representative images from Transwell assays with cells stained with
861 crystal violet comparing levels of invasion between doxycycline induced pCW57-VC and pCW57-UHRF1
862 MSC treated with DMSO or 150 µM amiloride. (H) Quantification of the number of MSC invaded across
863 the Transwell membrane from experiment shown in G. Each data point is mean ± s.d. of triplicate samples.
864 (I) Quantification of distance (pixels) migrated in scratch-wound assays for each of the OS cell lines treated
865 with DMSO or 16.4 µM BC 11 hydrobromide in SJSA-1, normalized to DMSO control. Each data point is
866 mean ± s.d. of ten measurements in triplicate samples. For all graphs: ns=not significant, ** $p < 0.01$, ***
867 $p < 0.001$, by unpaired two-tailed *t* test. (J) Model of UHRF1 oncogenic function in OS. In the absence of
868 RB or upon RB inactivation via hyperphosphorylation, activator E2Fs drive *UHRF1* transcription. The
869 resulting UHRF1 protein overexpression stimulates proliferation and uPA overexpression, aiding to
870 migration, invasion, and metastasis. For OS with CDK4/6 amplification, palbociclib treatment is an
871 effective way to reduce UHRF1 expression and result in decreased proliferation and migration.
872 Downstream of UHRF1, uPA inhibitors (e.g. amiloride, BC 11 hydrobromide) are attractive therapeutic
873 options to decrease migration and metastasis. For most OS (with or without *RB1* mutations), the
874 development of UHRF1-targeted therapeutics might result in beneficial decrease in both tumor growth
875 and pulmonary metastases.